

بِسْمِ اللَّهِ الرَّحْمَنِ الرَّحِيمِ



ISLAMIC UNIVERSITY OF TECHNOLOGY

**Automatic Lesion Segmentation of Breast Ultrasound Image:
An approach towards full automation**

A Thesis Presented to
The Academic Faculty
by

Rashid-Al-Mukaddim (102405)

Nafiul Islam (102408)

Fahim Ahmed Zaman (102410)

A dissertation

Submitted in partial fulfillment of requirement for the
Bachelor of Science in Electrical and Electronic Engineering
Academic Year: 2013-2014

Department of Electrical and Electronic Engineering

Islamic University of Technology (IUT)

A Subsidiary Organ of OIC

Gazipur, Bangladesh

A dissertation on,
**Automatic Lesion Segmentation of
Breast Ultrasound Image:
An approach towards full automation**

Approved By

Prof. Dr. Md. Shahid Ullah
Head of the Department
Department of Electrical and Electronic Engineering
Islamic University of Technology (IUT)
Gazipur-1704, Bangladesh.

Supervised by

Md. Taslim Reza
Assistant Professor
Department of Electrical and Electronic Engineering
Islamic University of Technology (IUT)
Gazipur-1704, Bangladesh.

Declaration of Authorship

This is to certify that the work presented in this thesis is the outcome of the analysis and investigation carried out by Rashid-Al-Mukaddim, Nafiul Islam and Fahim Ahmed Zaman under the supervision of Md. Taslim Reza in the Department of Electrical and Electronic Engineering (EEE), IUT, Gazipur, Bangladesh. It is also declared that neither of the thesis nor any part of this thesis has been submitted anywhere else for any degree or diploma. Information derived from the published and unpublished work of others has been acknowledged in the text and a list of references is given.

Authors

Rashid-Al-Mukaddim
Student ID: 102405

Nafiul Islam
Student ID: 102408

Fahim Ahmed Zaman
Student ID: 102410

Abstract

Breast cancer is the most common cause of death among patients. One of the main reasons is that the lesion is not identified in proper time to seek medical facility. The situation in Bangladesh is alarming as there is a huge female population in the rural areas who don't have proper medical access to detect the early stage of breast cancer.

We have tried our utmost to contribute to the development of a Computer Aided Diagnosis (CAD) system that will detect the tumorous lesion in the BUS (breast ultrasound) image automatically. The algorithm will be able to come up with a Region of Interest (ROI) which eliminates human intervention in this phase. ROI generation phase consists of Horizontal cut based on entropy information and calculation of directional gradient from automatically generated seed point. Finally, we segmented our ROI image by adopting two approaches; one using watershed segmentation technique and other using entropy filtering. The thesis concludes with the comparison among the two segmentation methods.

Keywords: Region of Interest (ROI), Entropy, Directional Gradient, SRAD Filtering, Watershed Segmentation, Binary thresholding, SOBEL Edge Detection

Acknowledgements

First and foremost, we offer gratitude to the Almighty Allah (SWT) for giving us the capability to do this work with good health.

We are grateful to our research supervisor, Md. Taslim Reza, for the support and guidance throughout our research at Islamic University of Technology (IUT) since September, 2013. He created a research environment for which we were able to explore many ideas without constraint. We have gained a wealth of knowledge and experience in science and engineering through his direction that is beyond value to our future endeavor. For these things, we give many thanks to him.

We are very grateful to Dr. S. Kaisar Alam, Visiting Professor, CBIM, Rutgers University, New Jersey, U.S.A. for providing us with Image Database. We are also very thankful to Minhaj Nur Alam, Lecturer, Department of EEE, IUT for extending help towards us whenever we were in need of it.

We would like to thank all the faculty members of the department of EEE, IUT for their inspiration and help.

Last but not the least, we are thankful to our family, friends and well-wishers for their support and inspiration. Without them it would never have been possible for us to make it this far.

Table of Contents

List of Figures	viii
List of Tables	x
Abbreviations	xi
1. Introduction	1
1.1 Present Scenario	1
1.2 Screening Techniques and Ultrasound Imaging.....	3
1.3 Thesis Objective	4
1.4 Thesis Organization.....	5
2. Ultrasound Imaging.....	6
2.1 Basics.....	6
2.2 Challenges	8
3. Literature Review.....	9
3.1 Introduction	9
3.2 Speckle reduction.....	9
3.3 ROI Detection	12
3.4 Segmentation	13
4. Automatic Region of Interest (ROI) Generation.....	18
4.1 Introduction	18
4.2 Existing Works and Problems	19
4.3 Proposed Method	19
4.3.1 Horizontal Cut based on Entropy Filtering	19
4.3.2 Seed Generation for Gradient Calculation	24
4.3.3 ROI Finalization using Directional Gradient.....	29
5. Automatic Lesion Segmentation from the derived ROI image	36
5.1 Introduction	36
5.2 Method 01	37
5.3 Method 02	48
5.4 Segmentation Results	50
5.4.1 Results from Method 01	51
5.4.2 Results from Method 02	52

6. Quantitative Evaluation of Segmentation Results	53
6.1 Area Error Metrics	53
6.2 Boundary Error Metrics.....	55
6.3 Materials	55
6.4 Result Analysis	59
7. Future Development and Conclusion	60
Bibliography.....	63

List of Figures

Figure 1.1 Average Number of New Cases per Year and Age-Specific Incidence Rates per 100,000 Population, Females, UK (Cancer Research UK)	2
Figure 2.1 Ultrasound beams are coming out sequentially from the Ultrasound transducer.....	7
Figure 2.2 Image reproduction from the Ultrasound beam	8
Figure 4.1 Original BUS Image	20
Figure 4.2 Entropy Filtered Image	20
Figure 4.3 Original BUS Image showing echogenicity	22
Figure 4.4 Entropy Filtered Image showing lesion.....	22
Figure 4.5 Entropy Filtered Image with three equal segments	23
Figure 4.6 Entropy Filtered Image showing regions.....	24
Figure 4.7 Entropy filtering on horizontal cut image.....	25
Figure 4.8 Binary image.....	25
Figure 4.9 Binary image depicting boundary connected regions	26
Figure 4.10 Binary image after deleting boundary connected regions.....	27
Figure 4.11 Binary Image with the Winning Region	28
Figure 4.12 Box showing Seed Point	29
Figure 4.13 Smaller Window Generation	30
Figure 4.14 Smaller Window	31
Figure 4.15 Gradient Image	32
Figure 4.16 Image with four quadrants.....	32
Figure 4.17 Rectangular ROI on the original image.....	33
Figure 4.18 Successfully Generated ROIs	35
Figure 5.1 Proposed Method 01	37
Figure 5.2 ROI Image	38
Figure 5.3 ROI Image before filtering.....	41
Figure 5.4 ROI Image after SRAD filtering.....	41
Figure 5.5 Topographic Relief Image	42
Figure 5.6 A Gray Scale Image.....	42
Figure 5.7 Flooding in Watershed Algorithm	43
Figure 5.8 Gray Scale Watershed Image.....	44
Figure 5.9 Color Mapped Watershed Image	44
Figure 5.10 Binary Image.....	45
Figure 5.11 3x3 Image Neighborhood	46
Figure 5.12 SOBEL Operator for x direction.....	46
Figure 5.13 SOBEL Operator for y direction.....	46
Figure 5.14 SOBEL Edge Detection	47
Figure 5.15 Segmented Image.....	47
Figure 5.16 Proposed Method 02	48
Figure 5.17 Entropy Filtering.....	48

Figure 5.18 Binary Image.....	49
Figure 5.19 Binary Image with the winning region.....	49
Figure 5.20 Detected Edge.....	50
Figure 5.21 Segmented Image.....	50
Figure 5.22 Segmented images using method 01.....	51
Figure 5.23 Segmented images using method 02.....	52
Figure 6.1 Areas corresponding to TP, FP, and FN regions	54
Figure 6.2 Case 01: (a) ROI image, (b) Watershed image, (c) Entropy image.....	56
Figure 6.3 Result comparison for case 01	56
Figure 6.4 Case 02: (a) ROI image, (b) Watershed image, (c) Entropy image.....	57
Figure 6.5 Result comparison for case 02	57
Figure 6.6 Case 03: (a) ROI image, (b) Watershed image, (c) Entropy image.....	58
Figure 6.7 Result comparison for case 03	58
Figure 7.1 Whole system overview of proposed methods.....	61

List of Tables

Table 4.1 Entropy Value and their respective regions	21
Table 6.1 Comparison between two proposed methods for case 01.....	56
Table 6.2 Comparison between two proposed methods for case 02.....	57
Table 6.3 Comparison between two proposed methods for case 03.....	58

Abbreviations

AD	Anisotropic Diffusion
BUS	Breast Ultrasound Image
CAD	Computer Aided Diagnosis
DOC	Dice Overlap Coefficient
FIR	Finite Impulse Response
FP	False Positive
HD	Hausdorff Distance
IOM	Institute of Medicine
JC	Jaccard Coefficient
MLP	Multilayered Perceptron
MRI	Magnetic Resonance Image
NN	Neural Network
PDE	Partial Differential Equation
ROI	Region of Interest
SRAD	Speckle Reducing Anisotropic Diffusion
TGC	Time Gain Compensation
TP	True Positive

Chapter 1

Introduction

Cancer is a group of diseases that cause cells in the body to change and grow out of control. Most types of cancer cells eventually form a lump or mass called a tumor, and are named after the part of the body where the tumor originates.

Breast cancer begins in the breast tissue that is made up of glands for milk production, called lobules, and the ducts that connect the lobules to the nipple. The remainder of the breast is made up of fatty, connective, and lymphatic tissues. Breast cancer typically produces no symptoms when the tumor is small and most easily cured. Therefore, it is very important for women to follow recommended screening guidelines for detecting breast cancer at an early stage. When breast cancer has grown to a size that can be felt, the most common physical sign is a painless lump. Sometimes breast cancer can spread to underarm lymph nodes and cause a lump or swelling, even before the original breast tumor is large enough to be felt.

1.1 Present Scenario

One in eight deaths worldwide is due to cancer [1]. Cancer is the second leading cause of death in developed countries and the third leading cause of death in developing countries. In 2009, about 562,340 Americans died of cancer, more than 1,500 people a day. Approximately 1,479,350 new cancer cases were diagnosed in 2009. In the United States, cancer is the second most common

cause of death, and accounts for nearly 1 of every 4 deaths [2]. Breast cancer is the most common, life-threatening cancer among American women [3]. The chance of developing invasive breast cancer at some time in a woman's life is about 1 in 8 (12%) [4, 5]. Breast cancer continues to be a significant public health problem in the world. Approximately 182,000 new cases of breast cancer are diagnosed and 46,000 women die of breast cancer each year in the United States [6]. In 2009, 192,370 new cases of invasive breast cancer were diagnosed among women in the United States [3]. Thus, the incidence and mortality of breast cancer are very high, so much so that breast cancer is the second leading cause of cancer death in women. The chance that breast cancer will be responsible for a woman's death is about 1 in 35 (about 3%) [4]. In 2009, about 40,610 women died from breast cancer in the United States [7]. Although breast cancer has very high incidence and death rate, the cause of breast cancer is still unknown [4]. No effective way to prevent the occurrence of breast cancer exists. Therefore, early detection is the first crucial step towards treating breast cancer. It plays a key role in breast cancer diagnosis and treatment. The technological boom in every aspect has made researchers to ponder over a screening tool that can be used to detect tumor in its developing stage, which can be used by the surgeons for further diagnosis.

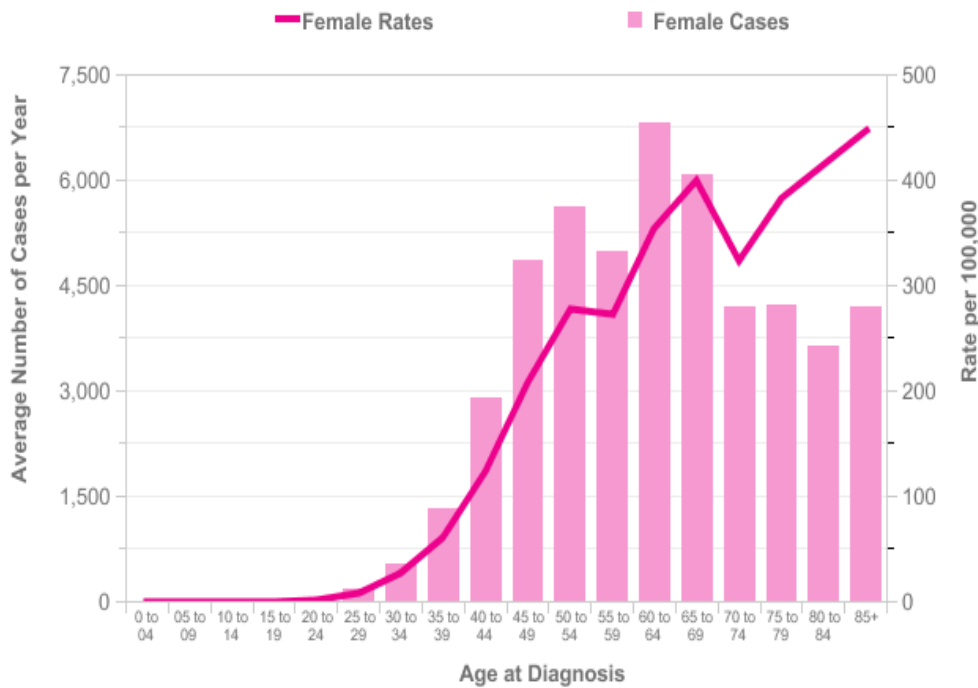


Figure 1.1 Average Number of New Cases per Year and Age-Specific Incidence Rates per 100,000 Population, Females, UK (Cancer Research UK)

According to the IOM (U.S. Institute of Medicine) report, an ideal breast screening tool [8]

- Has minimal health risk;
- Sensitive to tumors;
- Early cancer detection capability;
- Non-invasive and easy to perform;
- Cost effective, easy to understand & consistent;
- Provides minimum discomfort to patients

For detection of small tumor(s), a consistent contrast between tumor and normal breast tissues is required. Medical imaging methods have been applied to breast cancer detection with various degrees of success [8]. Early detection of cancers can reduce unnecessary biopsies in a drastic manner which will result in less hazards for the patients under diagnosis.

1.2 Screening Techniques and Ultrasound Imaging

Breast cancer screening is vital to detecting breast cancer. The most common screening methods are mammography and sonography. Ultrasound imaging has proved to be a valuable addition to mammography in the detection and classification of breast lesions [9]. Due to low specificity Mammography can detect false positives resulting in unnecessary biopsy operations. Also Mammography is ineffective in detecting breast cancer in adolescent women because of ongoing breast tissue formation in that age period.

Ultrasound (US) imaging technique is far superior to the other imaging modalities in many aspects. Firstly, Ultrasound is a non-invasive method for imaging causing almost no hazard for the patients undergoing the diagnosis; secondly, it is a very suitable for people of all classes, specially the developing countries as it is a very low cost diagnosis technique. Also another vital point that makes it superior to other techniques is that it does not expose the patients to any radiation so US imaging is very safe for the patients. Magnetic Resonance Imaging (MRI) is very widely used but still this test cannot be performed during

pregnancy or to a patient having heart problems due to application of a huge magnetic field. Ultrasound image can classify benign and malignant type of tumors which is another feature that puts US imaging above other imaging modalities. The dissemination of breast cancer disease is reported to increase rapidly due to the shortcomings in the currently used screening methods, where X-ray mammography is the widely used screening technique amongst MRI to detect breast tumors however it has been reported to have estimated false results for around 30% of women who have had a screening [10-11]. The considerable amount of false results obtained is noticeably the limitation of the present screening methods in analyzing dense breast tissue and the area where the tumor might be located close to the chest or under the arm and mainly the estimation of early stage tumors [12]. Keeping these issues in mind US imaging is capable of detecting less false detection which makes it efficient in detecting tumor lesions. Comparing with the other Computer Aided Diagnosis (CAD) available currently US imaging is more reliable and at the same time cost-effective. Ensuring maximum safety to the patients US imaging can be very helpful in classifying benign and malignant type of cancers. Developing countries and also countries possessing fewer resources will be able to facilitate the cancer detection using US imaging within their restraints.

1.3 Thesis Objective

The thesis mainly focuses on devising an automatic computer-aided system which will be capable of processing input ultrasound image. The main objectives of the thesis can be summarized as follows:

- Automatic Region of Interest (ROI) generation from the original image for eliminating the operator dependency of manual delineation of ROI and facilitating easier segmentation;
- Devising a reliable segmentation method for successfully segment the ROI image;
- Finally, integrate this two systems for designing an effective and reliable breast cancer detection CAD system.

1.4 Thesis Organization

The thesis has been arranged in the following way-

- In **Chapter 2**, the basic theory behind Ultrasound Imaging Modality is discussed. This chapter emphasizes on the image acquisition using ultrasound machines and several inherent features of BUS image.
- In **Chapter 3**, focus is provided on reviewing existing works in three important steps in BUS image processing: Noise Reduction, ROI Detection and Segmentation.
- In **Chapter 4**, an automatic ROI generation method is proposed. Details of the generation process are discussed.
- In **Chapter 5**, two different approaches for segmenting the extracted ROI image are discussed. Successful results along with detailed methodology are provided.
- In **Chapter 6**, performance evaluation is carried out for the segmented images using statistical metrics.
- In **Chapter 7**, we have provided the concluding remarks about our work and our future plans with the thesis.

Chapter 2

Ultrasound Imaging

2.1 Basics

The term 'Ultrasound' relates to frequency or wavelength. There are three region of frequency range-'subsonic', 'sonic' and 'ultrasonic'. The acoustic wave that fall in the frequency range of human ear (20Hz to 20 kHz) is called sonic. The waves having a frequency range less than 20Hz are subsonic and importantly the waves having frequency range greater than 20kHz are regarded as 'ultrasonic' or 'ultrasound'. Here we will use ultrasound and ultrasonic interchangeably.

Ultrasound is used in the clinical applications extensively these days. It is noninvasive, portable and more over the cost of clinical treatments with ultrasound technology is less expensive and affordable. It is not only possible to visualize the anatomy or morphology with ultrasound imaging but can also measure or predict the almost all kind of function by means of blood. Nowadays it is extensively used in fetal imaging, carding imaging, breast cancer detection, and detection of benign and malignant tissue in the human body. Though the ultrasound frequency range starts from 20 kHz, in clinical

applications we use typically a range from 1MHz to 15MHz. The typical velocity of ultrasound in the human tissue is 1540 m/s.

The ultrasound is generated by a piezoelectric crystal. This piezoelectric crystal is embedded in the transducer which acts both as transmitter and receiver in the ultrasound imaging process. The crystal deforms under the influence of an electric field and vice versa.



Figure 2.1 Ultrasound beams are coming out sequentially from the Ultrasound transducer

Ultrasound is longitudinal mechanical wave. In case of longitudinal wave the displacement of the particles in the medium is parallel to the motion of the wave. As the ultrasound is generated from the piezoelectric crystal, a mechanical wave is generated from the application of an electrical signal (electric field). The ultrasound that is produced from the transducer passes through the tissues and tissue boundaries. As a result reflection, refraction, diffraction of the acoustic wave occurs in the tissue boundaries. At the boundaries of the tissues, the energy of the wave is slightly reflected back to the transducer and the rest of the energy is transmitted through the tissue boundary. The reflected waves are detected by the transducer and the time between the signal transmission and reception in the transducer is calculated to reveal the position and the depth of the tissue boundaries. This process is repeated again and again until the entire image is found. In this

way the entire image can be formed within a fraction of second leading to real time imaging [2].

Figure 2.2: In the first figure one on the left, the ultrasound wave is going through the tissue, while some portion of the wave is reflected from the tissue boundaries and the rest are transmitted again through the tissue.

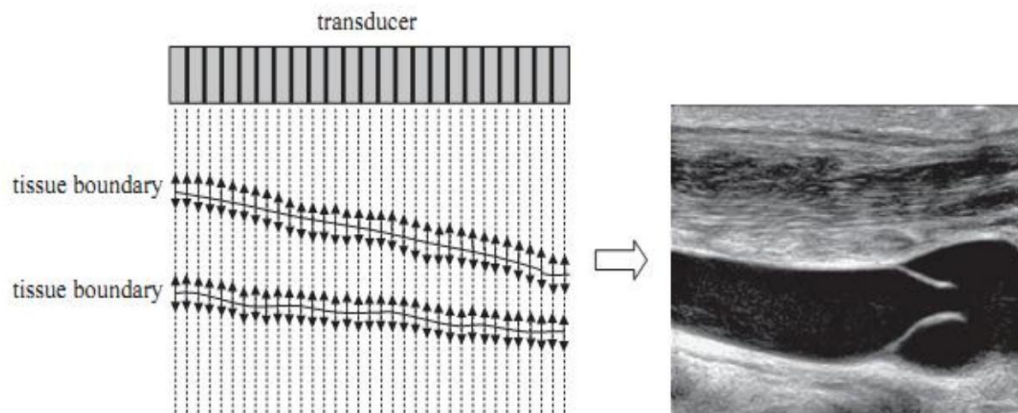


Figure 2.2 Image reproduction from the Ultrasound beam

Second figure on the right shows an image that can be obtained using ultrasound (typically a B-Mode scan). Image is reproduced from [2].

2.2 Challenges

Though Ultrasound imaging is superior in terms of expense and health hazard, but its inherent noise artifacts make image analysis complex. In the course of working with US imaging the challenges we faced are -

- Speckle Noise
- Attenuation
- Shadow Artifacts
- Low Contrast
- Blurry Boundaries between the objects and background
- Low Signal/Noise ratio

Chapter 3

Literature Review

3.1 Introduction

Since the underlying molecular mechanism of this disease still remains unknown, early detection and diagnosis are very essential in reducing the mortality. More and more emphases are given on early detection and diagnosis of breast cancer. Currently, breast ultrasound (BUS) imaging is a valuable method in early detection and classification of breast lesions [13].

Researchers working on segmentation of BUS images mainly emphasize on dividing the process into some parts such as Speckle Reduction, Region of Interest (ROI) detection, Segmentation. After these comes the diagnosis and error comparison.

3.2 Speckle reduction

Even though, in some cases the speckle are essential information to track features, many cases the speckle noise deteriorates the image quality, degrades the fine details and edge definition. It also limits the contrast resolution, limiting the detectability of small, low contrast lesions in body. Speckle is

always considered as a primary source of medical ultrasound imaging noise, and it should be filtered out.

The Mean Filter is a simple one and does not remove the speckles but averages it into the data. Generally speaking, this is the least satisfactory method of speckle noise reduction as it results in loss of detail and resolution.

Median filtering in medical de-noising is used for the inhibition of salt and pepper noise [14]. The filter median is a simple nonlinear operator that replaces the middle pixel in the window with the median value of its neighbors. Hybrid median filter [15] that removes impulse noise while preserving edges as compared to the median filter this has better corner preserving characteristics. This filter preserves edges much better than median filter [16].

Speckle noise is an inherent in medical ultrasound images; the most widely used median filter model speckle noise as multiplicative independent identical Rayleigh Distribution with little concerns about its high correlation. Hence they perform poor when it comes to real ultrasound images.

Wiener filter performs smoothing of the image based on the computation of local image variance. When the local variance of the image is large the smoothing is little, on the other hand if the variance is small, smoothing will be better.[17] Wiener filter can be used as de-correlator of speckle, which makes its distribution more in reflectivity. If reflectivity is reasonably assumed to be corrupted by multiplicative noise then an adaptive ML estimation approach is utilized to eliminate such noise [18].

Lee et al [19] preprocessed US images by a 4x4 median filter to reduce the speckle noise & to enhance features. For removing noise or spot, image regularization problem was considered. Mean Variance Model was used to solve the problem for smooth image by utilizing the global variation framework. But this filter is incapable of removing high frequency noise and also it cannot remove noise in high and low variance regions.

An improved version of lee filter known as enhanced lee filter (Enh Lee) which eliminates the demerits of lee filter mentioned above [20]. Lopes et al. [21]

expands the Lee et. Al approaches by adapting to local heterogeneity, based on $CI(x,y)$ which represents the effective descriptor of textural information and image homogeneity, the image is split into three regions of different filtering ,using thresholds and one of the thresholds determines how much of the image is to remain unfiltered.[22]

Perona and Malik proposed a method called anisotropic diffusion equation (P-M equation). It smooth within the region also has a very good edge preserving property. This filtering method is based on diffusion equation and is a new method in recent years. This method originated from the thermal diffusion equation. First, image feature should be introduced into the diffusion equation. Then designing appropriate diffusion coefficient to control the diffusion behavior result in the diffusion is smaller along the gradient direction and bigger along the vertical of the gradient direction [23].

Rafael et al [29] used Band Pass Filtering to provide valuable information on region transitions of US images while rejecting most of the noise components. The filter is obtained using the McClellan transformation over a 1-D FIR filter. Gaussian Smoothing is also used to reduce the influence of noise. Gaussian smoothing is performed over a series of iterations. The Gaussian filter consists of a 5x5 square matrix. Filter size and standard deviation is constant on all iterations.

Xu Liu et al applied Anisotropic Diffusion Non-linear filter is applied to smooth the noise. Yu and Acton developed a diffusion approach better suited to speckle noise removal. AD filter works well for images corrupted with additive noise. In case of images with speckle noise, Speckle Reducing Anisotropic Diffusion (SRAD) filter is approved [76]. In SRAD diffusion constant is proposed in terms of 'Instantaneous Coefficient of Variation' as a function of the local gradient magnitude and laplacian operators [24]. The demerits of this filter include that it requires a lot of computation time. To improve upon the operation of the filter in [2] a DPAD filter is proposed which makes the computation time less than SRAD filter. In ultrasound images of artery, linear features are important. For thin and linear features SRAD filter tends to broaden. In order to remove this disorder reg-SRAD filter is used.

The geometric filter of Crimmins [26], and improved by Busse et al. [27], is derived from geometric concepts. As noted in [22] the geometric filters on application of real ultrasound images remove most of the speckle, also noted that the computational complexity of geometric filters is lowest at the expense of lower speckle reduction capability.

Yap et al used a hybrid filtering approach that combines the strength of nonlinear diffusion filtering to produce edge-sensitive speckle reduction, with linear filtering (Gaussian blur) to smooth the edges and to eliminate over segmentation. Subsequent to hybrid filtering, multi-fractals are used to further enhance the partially processed images.

3.3 ROI Detection

ROI selection is crucial for segmentation because it reduces the computational area and time. It also makes it easier for the computing machine to find the lesion and detect the lesion boundary. In the papers [28, 29, 30] segmentation algorithm concludes ROI detection.

In the paper [28], Level Set Method is used to obtain the ROI. Level Set method is a hybrid speed function method which considers a boundary and region information for masses segmentation.

In the paper [29], ROI selection was automatic. Object Suppressing Operation is used to obtain binary images containing ROI and in most cases, small misclassified isolated objects are considered as noise.

A rule based approach is used to identify important ROIs by Yap et al. ROI is detected automatically. The first criterion for the identification of lesions is the size of the segments. The suspect lesions are identified as the largest segments among the likely multiple segments that result from applying the single threshold segmentation. It is observed that 95% of tumors are located at the upper regions of the images. Some researchers select the ROI manually as in [31, 32, 33, 34] and then try to find the contour/edge of the lesion.

3.4 Segmentation

The principal segmentation challenges pertain to characterizing the textured appearance and geometry of a cancer relative to normal tissue, and accommodating artifacts such as the possibly strong attenuation across an image and shadowing, as well as the “fuzziness” of cancerous mass boundaries which makes border delineation difficult. Importantly, the studies of Stavos [35]-[37] have greatly influenced the design of algorithms for breast mass detection. Interestingly, no significant work has looked at the screening case, i.e., most work has assumed the presence of a, typically single, suspicious mass.

Many techniques have been developed for BUS segmentation. They are categorized into histogram thresholding, region growing, model-based (active contour, level set, Markov random field) and machine learning.

Simple histogram thresholding [38, 39] or region-growing algorithms [40, 41] can find the preliminary lesion boundary. In a histogram thresholding method, an intensity threshold is chosen at the valley of the image histogram to separate the image into background and foreground. For a region growing method, a region is grown from the seed point (start point) by adding similar neighboring pixels.

Although efficient, these methods cannot generate a precise boundary because their over-simplified concepts and the high sensitivity to noise. However, they can serve as an intermediate step to provide a rough contour [40] or can be combined with post-processing procedures such as morphological operations [38, 39, 42], disk expansion [43], Bayesian neural network [45], function optimization [44] etc.

Horsch et al. [47] presented a method involving thresholding a preprocessed image that has enhanced mass structures. Comparison is made of a partially automatic and fully automatic version of the method with manual delineation on 400 cases/757 images (124 “complex” cysts, 182 benign masses, and 94 malignant masses). They compute four image based features (shape, echogenicity, margin, and posterior acoustic behavior) defined respectively in

terms of the depth-to-width ratio, autocorrelation, “normalized radial gradient,” and comparison of gray levels, to test their effectiveness at distinguishing malignant and benign masses. This method was further evaluated in [48] and [49] to assess the advantages of different features using linear discriminant analysis where the best two features were found to be the depth-to-width ratio (shape) and normalized radial gradient (margin). In later work aimed at further automating the method Drukker et al. [50] extended this work to include mass detection by proposing to first filter the images with a radial gradient index filtering technique. The method was tested on the same database as in [47] and [48]. They showed that 75% of lesions were correctly identified.

Neural network (NN) based methods have proved to be popular in this area. These aim to make a classification decision based on a set of input features. For instance, Chen et al. [51] presented a NN approach where input features were variance contrast, autocorrelation contrast, and the distribution distortion in the (Daubechies) wavelet coefficients and a multilayered perceptron (MLP) neural network with one hidden layer was trained by error back propagation. The method was applied to a database of 242 cases (161 benign, 81 carcinoma) giving a sensitivity of 98.77% and specificity of 81.77%. They strongly argued that image texture was an important component that made their method successful.

Huang and Chen [52] proposed an approach that integrates the advantages of NN classification and a watershed segmentation methods to extract contours of a breast tumor from ultrasound images. The main novelty of this work is in the preprocessing step which helps effectively the watershed algorithm by means of a reasonably good selection of markers. The authors proposed to use a self-organizing map (SOM) texture based NN in order to select adaptively (i.e., locally) from a set of nine pre-defined filters the appropriate preprocessing filter to use. Their method was tested on a database of 60 images (21 benign, 39 carcinomas), 40 used for training, 20 for testing. Measures of contour difference and area difference between the method and manual delineation were evaluated although strong conclusions cannot be drawn from this evaluation.

Xiao et al. [54] presented an expectation maximization method that simultaneously estimates the attenuation field at the same time as classification

of regions into different (intensity based) regions. The number of regions (classes) needs to be specified, which in the intended application is not a strong limitation. That method was tested on experimental data with different time gain compensation (TGC) settings to show that their approach gave consistent segmentations under different TGC settings but has not undergone a large clinical assessment. This method is compared to that of Boukerroui in [53].

Madabhushi and Metaxas [46] combined intensity, texture information, and empirical domain knowledge used by radiologists with a deformable shape model in an attempt to limit the effects of shadowing and false positives. Their method requires training but in the small database. Using manual de-lineation of the mass by a radiologist as a reference, and the Hausdorff distance and average distance as boundary error metrics, they showed that their method is independent of the number of training samples, shows good reproducibility with respect to parameters, and gives a true positive area of 74.7%. They also argued that it has automation advantages over the work of Horsch et al. [47].

Boukerroui et al. [53] used a Markov random field to model the region process and to focus on the adaptive characteristics of the algorithm. Their method introduced a function to control the adaptive properties of the segmentation process, and took into account both local and global statistics during the segmentation process. A new formulation of the segmentation problem was utilized to control the effective contribution of each statistical component. The merit of MRF modeling is that it provides a strong exploitation of the pixel correlations. The segmentation results can be further enhanced via the application of maximum a posteriori segmentation estimation scheme based on the Bayesian learning paradigm.

Watershed based approaches have shown promising performances for ultrasound image segmentation. The methods consider image as topographic surface wherein the grey level of a pixel is interpreted as its altitude. Water flows along a path to finally reach a local minimum. The biggest challenge for such methods is over segmentation; to address the problem; many approaches have been proposed and can be categorized into two types: marker controlled and cell competition.

Marker controlled methods inundate the gradient landscape of image and define watersheds when the flooding of distinct markers rendezvous with each other. Hence, the identification of makers is very crucial in solving the over-segmentation problem. The method proposed in [55] was a texture-based approach that selected the marker candidates as seeds for the water level immersion. A self-organization map was trained to identify the texture of lesions as the flooding markers. Distinctively, the method in [56] adopted a thresholding and morphological operation scheme to seek flooding markers. It required a heuristic estimation of the best thresholding of markers to achieve the task of lesion delineation.

Cell competition approaches, on the other hand, alleviate the over-segmentation problem in a different way. A two-pass watershed transformation [57] was performed to generate the cell tessellation on the original ultrasound image or ROI. In this method, a competition scheme based on the cell tessellation was carried out by allowing merge and split operations of cells. The cost function was devised to characterize boundary saliency and regional homogeneity of an image partition, and it drove the competition process to converge to a prominent component structure. However, neither marker controlled nor cell competition approaches guarantee to solve the over segmentation problem completely [58].

Although some of the previous methods can be applied in 3-D, the literature on 3-D is less extensive. For instance, Chen et al.[59], Chang et al.[60]–[62], and Sahiner et al.[63] take a deformable active contour approach. Chang et al. [60] applied an active contour which uses intensity and intensity variance information. The method was tested on eight tumors (four benign, four malignant) with volume estimates compared with estimates by manual delineations. Using the match rate as a performance metric, the average match rate was about 95%.

Sahiner et al. [63] compared 2-D and 3-D intensity gradient active contour segmentation based methods, the active contour initialized by hand, and with algorithm parameters determined empirically. Having found the segmentation solution, depth-to-width ratio, a posterior shadowing feature measure, and 72 texture features based on co-occurrence matrix analysis were computed

around the boundary for each 2-D slice and linear discriminant analysis used to classify volumes. Four radiologists graded the volumes in terms of perceived malignancy on a scale 1–10. They showed that the radiologist and computer-based methods were not statistically different in classification (versus average for radiologists). However, they did not look at the accuracy of segmentation in depth and recognized that this was an area of possible improvement.

Chapter 4

Automatic Region of Interest (ROI) Generation

4.1 Introduction

BUS images contain a lot of different structures (connective tissue, fat, muscles, etc.) and the lesion area is usually small compared to the entire image, finding a region of interest (ROI) is quite helpful for improving the speed and accuracy of segmentation. [31]

Many existing BUS image segmentation methods have been developed based on a manually selected ROI, not on the whole image. Such a requirement hinders full automation of BUS image segmentation. In this chapter, we describe the development of an automatic ROI generation method that facilitates full automation of BUS image segmentation.

There are two typical ROI definitions: one defines ROI as the rough contour or initial contour of the lesion, while the other defines ROI as a rectangular region containing both the lesion and some background information.

In our proposed method, we adopt the latter definition that is our automatically generated ROI is a rectangular region. Therefore, this ROI generation method

can be utilized by any other segmentation method as a preprocessing step since it only cuts the redundant background while keeping the lesion and nearby surrounding tissues untouched.

4.2 Existing Works

There are many existing methods which aim to achieve automation in the ROI generation phase. Some of these are: Automatic ROI production by a supervised texture classification method [64], ROI generation using texture features and spatial characteristics [65], ROI generation using self-organizing map neural network [66] etc. In next section we propose a novel ROI generation method of BUS image.

4.3 Proposed Method

In our proposed method we considered texture information as well as spatial characteristics of BUS image. Our automatic ROI generation method involves three major steps:

- Horizontal Cut based on Entropy Filtering
- Seed Generation for Gradient Calculation
- ROI Finalization using Directional Gradient

4.3.1 Horizontal Cut based on Entropy Filtering

We first applied entropy filtering on BUS image. Entropy is a textural feature and can be defined as a measure of randomness [67]:

$$Entropy = -\sum_{i=0}^{L-1} p(x_i) \log_2 p(x_i) \quad 4.1$$

In equation 4.1, x is a random variable

$p(x)$ is the histogram of the intensity levels

L is the number of possible intensity levels.

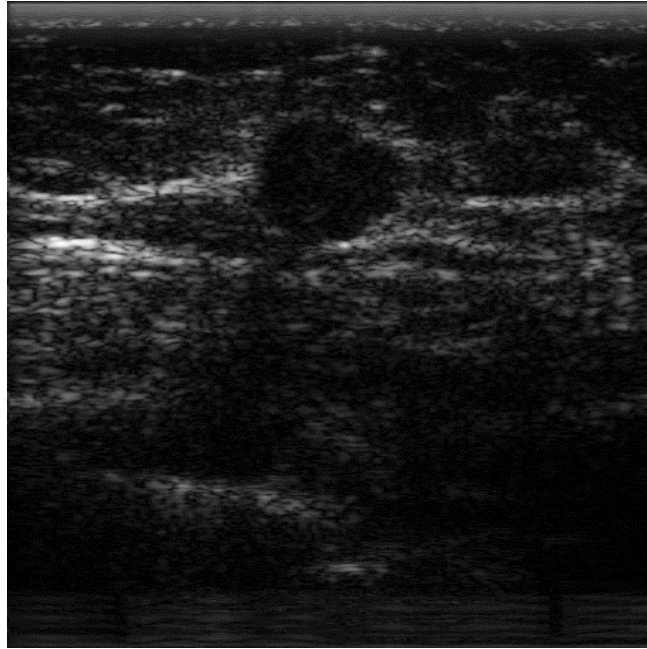


Figure 4.1 Original BUS Image

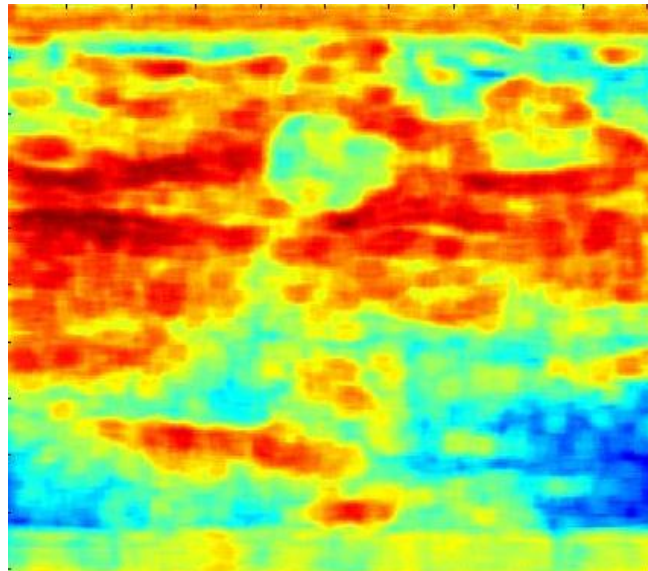


Figure 4.2 Entropy Filtered Image

From the entropy filtered images, we observed that the entropy values are different for different regions. We categorized entropy values based on these regions. These values are tabulated in Table 4.1.

Table 4.1 Entropy Value and their respective regions [68]

Regions (in terms of location)	Regions (in terms of echogenicity)	Entropy Value	Comments
Boundary of the lesion	Hyperechoic	>6.5	This is general for all test images
Inside the lesion	Anechoic	5~6	Varies with images but mostly the entropy value is lesser than the values around the lesion
Rest of the image	Mostly hypoechoic	5~6.5	With some anechoic regions

The entropy values in the dark (anechoic) region inside the lesion vary from 3 to 5. The white (hyperechoic) region found near the boundary of the lesion has very high entropy values ranging from 6 to 7.5. The rest of the image with mostly gray regions (hypoechoic) has values from 5 to 6.5. The regions can be seen in the original BUS image shown in Fig. 4.1. Corresponding entropy image in Fig. 4.2. Low entropy values indicate that randomness is small inside the lesion, i.e. the grayscale-intensity values within the lesion do not vary much compared to that of the region near boundary. Due to high variation of grayscale-intensity values, entropy is higher near boundary. These echogenic regions are depicted in Fig 4.3 and Fig 4.4. We used this information for our horizontal cut.

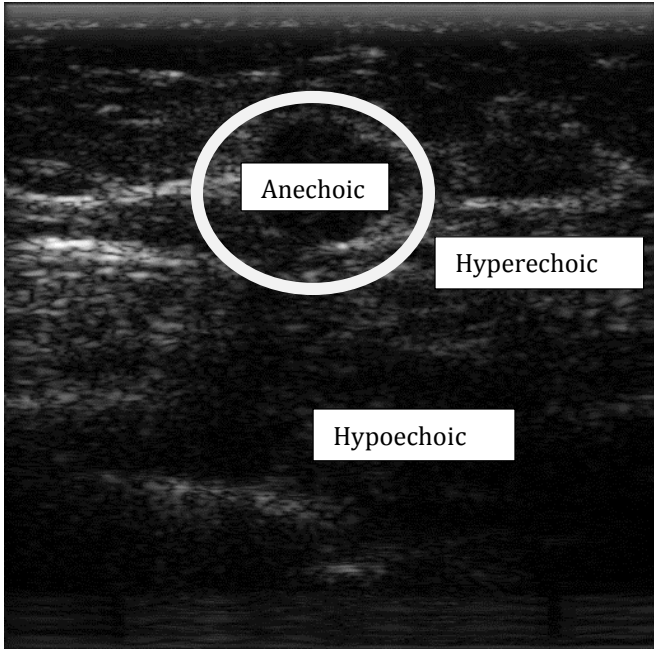


Figure 4.3 Original BUS Image showing echogenicity

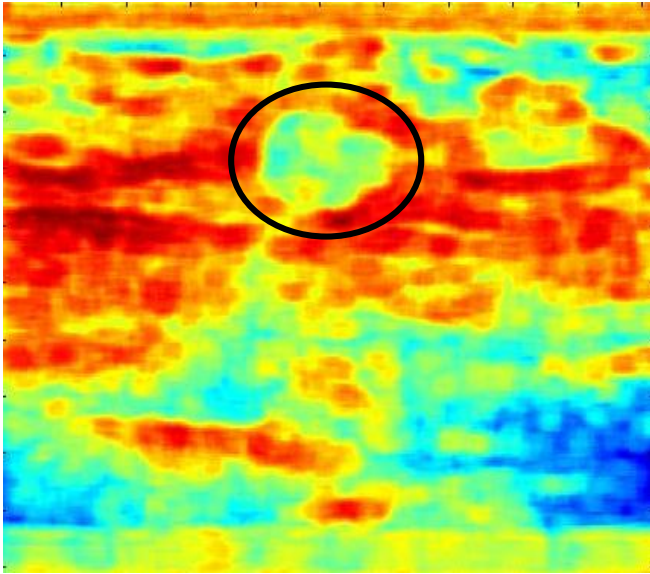


Figure 4.4 Entropy Filtered Image showing lesion

In our next step we divide our image three equal segments as shown in Fig 4.5. In this step our main focus is to discard the segment which has the lowest entropy value among the three and preserve the segments with higher entropy values. Our motivation behind this approach lies in the discussion above that region surrounding the lesion has higher entropy value so preserving segment with higher entropy values means preserving the lesion and discarding the unnecessary regions.

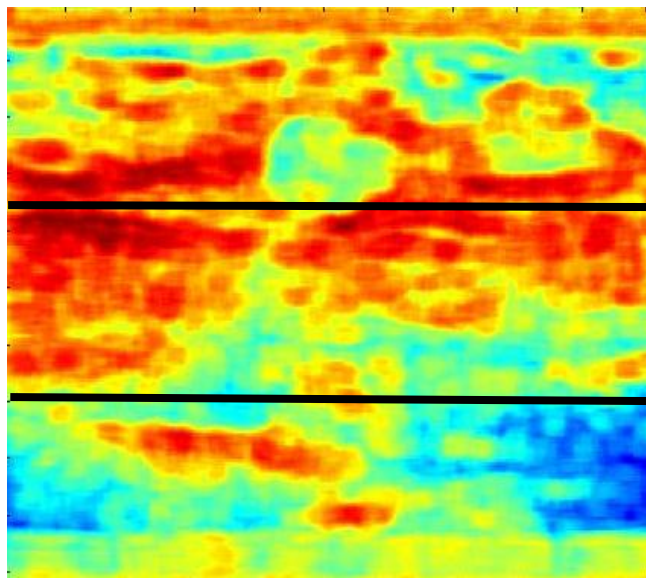


Figure 4.5 Entropy Filtered Image with three equal segments

After dividing the image into three equal segments we formed two regions as shown in Fig 4.6. We calculated total entropy of region 1 and region 2. If the entropy value of region 1 is greater than the entropy value of region 2 then we discarded segment 3. Again if the entropy value of region 2 is greater than the entropy value of region 1 then we discarded segment 1. Thus we achieve an output image with one segment less than the original image. In this way, we achieve horizontal cut of the original image based on entropy filtering.

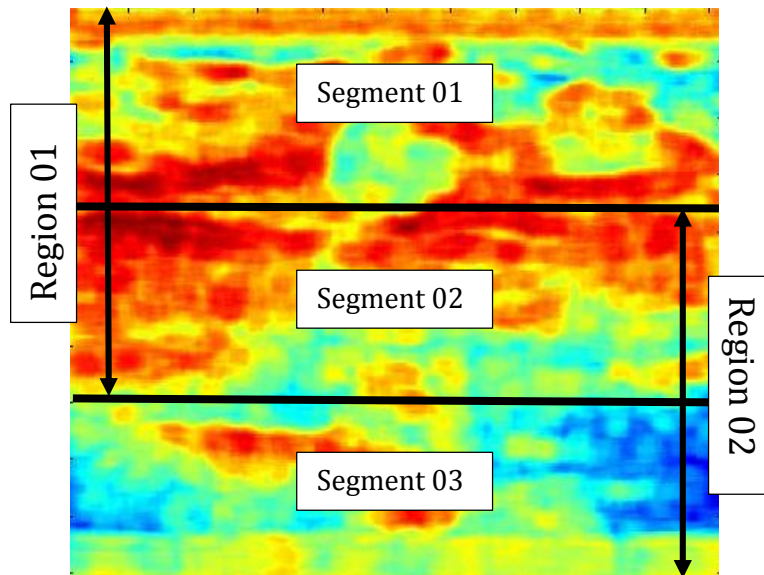


Figure 4.6 Entropy Filtered Image showing regions

4.3.2 Seed Generation for Gradient Calculation

Step 01: Binary Image Formation

We firstly apply entropy filtering on the horizontal cut image. Then we transformed our entropy filtered image into binary image using entropy thresholding. For our thresholding, we used following equation for threshold determination:

$$EnTh = \frac{MaximumEntropy + MinimumEntropy}{2} \quad 4.2$$

Fig 4.7 shows the entropy filtered image and Fig 4.8 shows corresponding binary image.

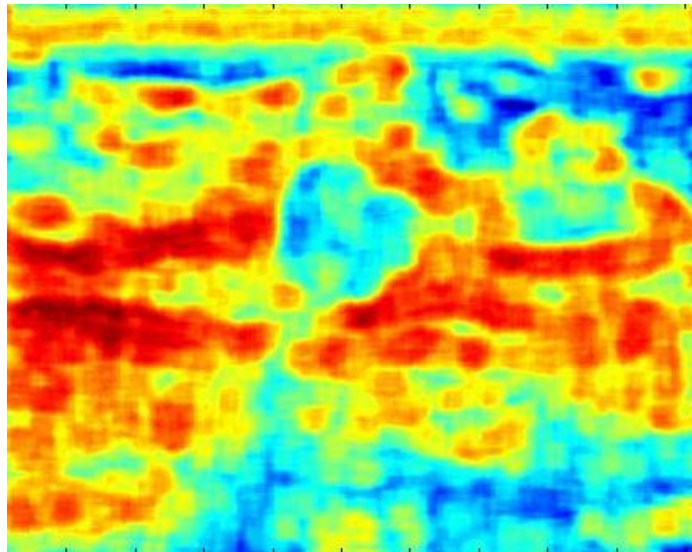


Figure 4.7 Entropy filtering on horizontal cut image



Figure 4.8 Binary image

Step 02: Deleting Boundary Connected Region

Subcutaneous fat, glandular tissue, and skin typically appear in the upper portion of the image [46]. Also, the shadowing region appears in the posterior part of the image [69]. We observed that these regions are generally boundary connected and occupies a large area. Fig 4.9 depicts these boundary connected regions. Thus eliminating boundary connected region will leave us potential lesion region. In this step, we used the technique mentioned in [70]. In this technique, a center window is used to evaluate every boundary region. If a region has no intersection with the center window and it is connected with any of the 4 image boundaries, this region is deleted from the lesion candidate list. The resultant image is shown in Fig 4.10.



Figure 4.9 Binary image depicting boundary connected regions



Figure 4.10 Binary image after deleting boundary connected regions

Step 03: Ranking the rest regions

Now the rest regions are either not connected with the boundary or they have an intersection with the image center window. Then we ranked the rest regions which are potential candidates of the lesion region. We considered two arguments here:

1. Finding the region with highest area
2. Finding the region nearest to the image center

We used the following ranking function from [31] with slight modifications:

$$S_n = \frac{A(n)}{d(c_n, c_o)} \quad 4.3$$

In this equation 4.3,

A (n)= Area of the nth region;

n=1, 2, 3.....k;

k =number of regions;

$d(C_n, C_o)$ =Distance between Center of the n th region, C_n to the center of the image, C_o .

The region with the maximum value from the ranking function marks our winning region for lesion. The winning region is shown in Fig 4.11.

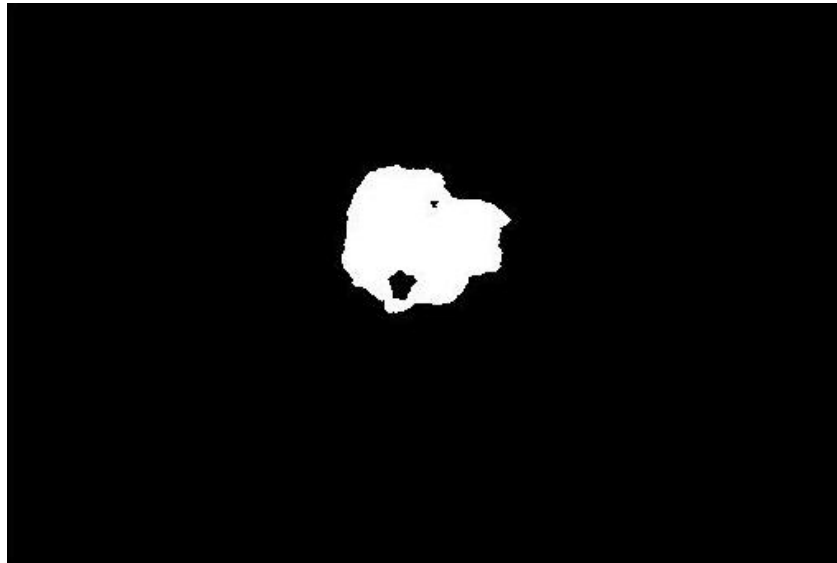


Figure 4.11 Binary Image with the Winning Region

Step 04: Determining the Seed Point

Let, R is the winning region from our ranking step, let x_{max} and x_{min} be the maximal and minimal horizontal coordinates of R , and let y_{max} and y_{min} be the maximal and minimal vertical coordinates of R , respectively. Then

$$X_{seed} = \frac{x_{max} + x_{min}}{2} \quad 4.4$$

$$Y_{seed} = \frac{y_{max} + y_{min}}{2} \quad 4.5$$

Generated seed point is shown in Fig 4.12. This seed point is used for further calculation.

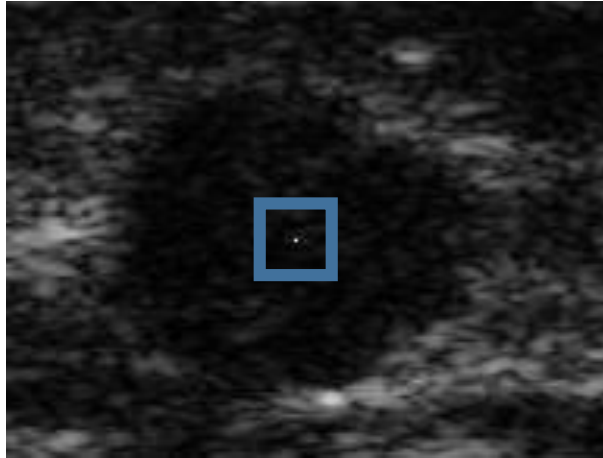


Figure 4.12 Box showing Seed Point

4.3.3 ROI Finalization using Directional Gradient

In this section, we finalize our ROI by calculating directional gradient. The gradient of an image f in the location (x, y) is defined as

$$\nabla f \equiv \text{grad}(f) \equiv \begin{bmatrix} g_x \\ g_y \end{bmatrix} \equiv \begin{bmatrix} \frac{\partial f}{\partial x} \\ \frac{\partial f}{\partial y} \end{bmatrix} \quad 4.6$$

Thus the gradient of an image requires computing the partial derivatives at every pixel location of the image. Since we are dealing with digital images, a digital approximation of the partial derivatives over a neighborhood about a point is required. The equation 4.6 can be discretely approximately as follows:

$$g_y = \frac{\partial f(x, y)}{\partial y} = f(x, y+1) - f(x, y) \quad 4.7$$

$$g_x = \frac{\partial f(x, y)}{\partial x} = f(x+1, y) - f(x, y) \quad 4.8$$

Using equation 4.7 and 4.8 in a modified way, we calculated directional gradient along 360 degrees taking seed point as center for finalizing our ROI.

Step 01: Smaller Window Generation

For our directional derivate calculation, we have used smaller rectangular window for the better approximation of the boundary. Smaller window eliminates chance of false boundary detection.

Let,

$Dy+$ = Perpendicular Distance of Image Boundary from the Seed Point in positive vertical direction

$Dy-$ = Perpendicular Distance of Image Boundary from Seed Point in negative vertical direction and Dx be the horizontal length of the image.

Then

Length of the rectangular window = Dx ;

*Breadth of the rectangular window = $2 * Dy$;*

$Dy = \min(Dy+, Dy-)$;

Figure 4.13 depicts this conventions mentioned and Fig 4.14 shows the smaller window generated for further calculations.

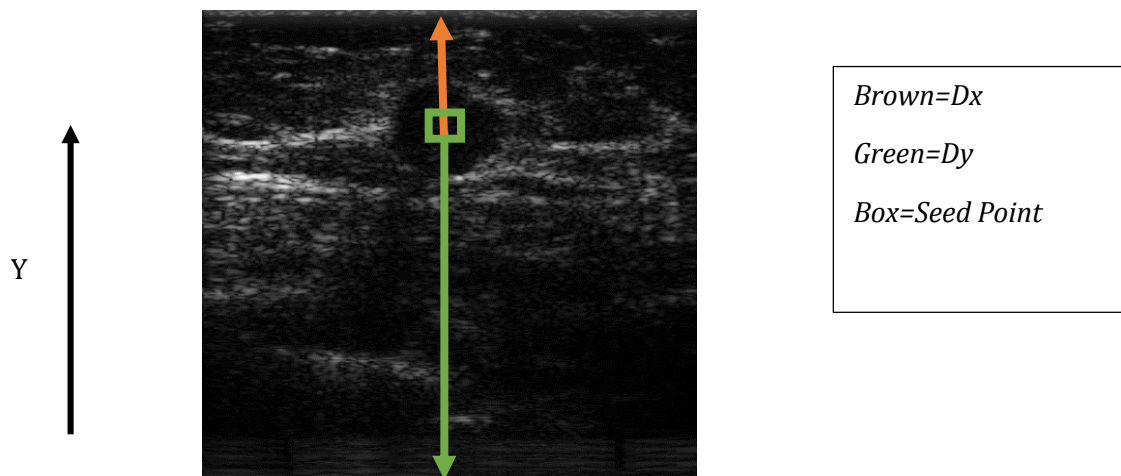


Figure 4.13 Smaller Window Generation

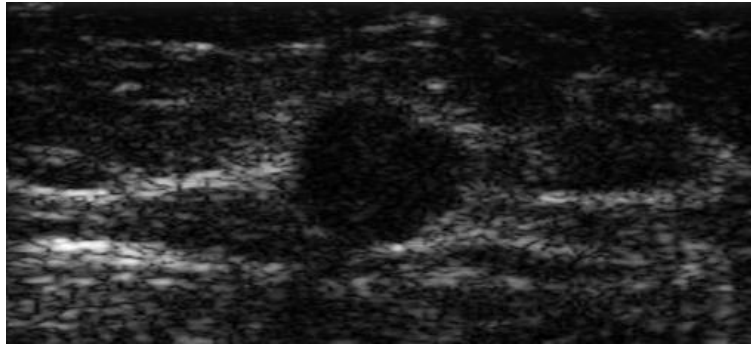


Figure 4.14 Smaller Window

Step 02: Gradient Calculation along 360 degree

Usually derivative calculation provides good result in boundary detection in noise-free image which is a very deviant case from ultrasound image. Here, we use derivative to obtain a preliminary contour serving as the intermediate result for ROI generation.

Before derivate calculation, we applied median filtering on the image to suppress speckle noise. We did not pay too much attention on noise suppression step as we are using directional derivate to approximate the boundary, not segmenting it.

To determine gradient of a pixel, $grad(j)$ for in a direction $\emptyset(i)$ we have used the following equation

$$grad(j) = |q1(j) - q2(j)| \quad 4.9$$

In equation 4.9,

j = number of pixels of the image;

$q1(j)$ = sum of next n no. of pixel intensities from the pixel under consideration, $p(j)$;

$q2(j)$ = sum of previous n no. of pixel intensities from the pixel under consideration, $p(j)$;

n = number of pixels considered for the calculation.

In our algorithm we found $n=8$ yielded good outcome. We have used this technique of pixel summation to suppress the noise effect of the ultrasound

image. Then, we determined 1st, 2nd and 3rd maximum value of gradients in all directions. Finally we achieve a rough boundary by calculating medians among the top three gradients in each directions. Fig 4.15 shows our gradient image showing the rough boundary.

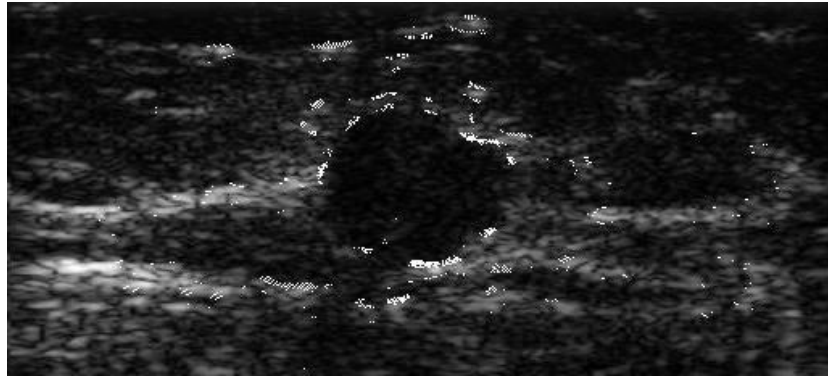


Figure 4.15 Gradient Image

Step 03: Final ROI Cut

For our final ROI cut, we divided our image into four quadrants as shown in Fig 4.16. Generally, we observed that the irregularity in the shape of breast lesion can be closely correlated with oval shape. This is our motivation behind choosing such quadrants as depicted in Fig 4.16.

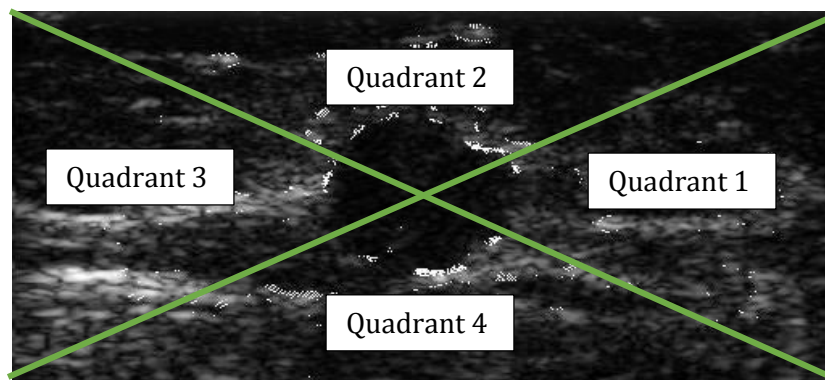


Figure 4.16 Image with four quadrants

From the set of gradient points in quadrant 1, we determined the average among those points and used the value as our radius of ROI in positive x direction. We purposefully added an offset of 15 pixels in order to make sure that the lesion is completely covered by ROI. The same procedure is repeated for other three quadrants. Thus we determine the average radius of our ROI centering from our original seed point.

Using this radius in four directions, we cut off our final Region of Interest. The result of the automated generated ROI is shown in Fig 4.17.

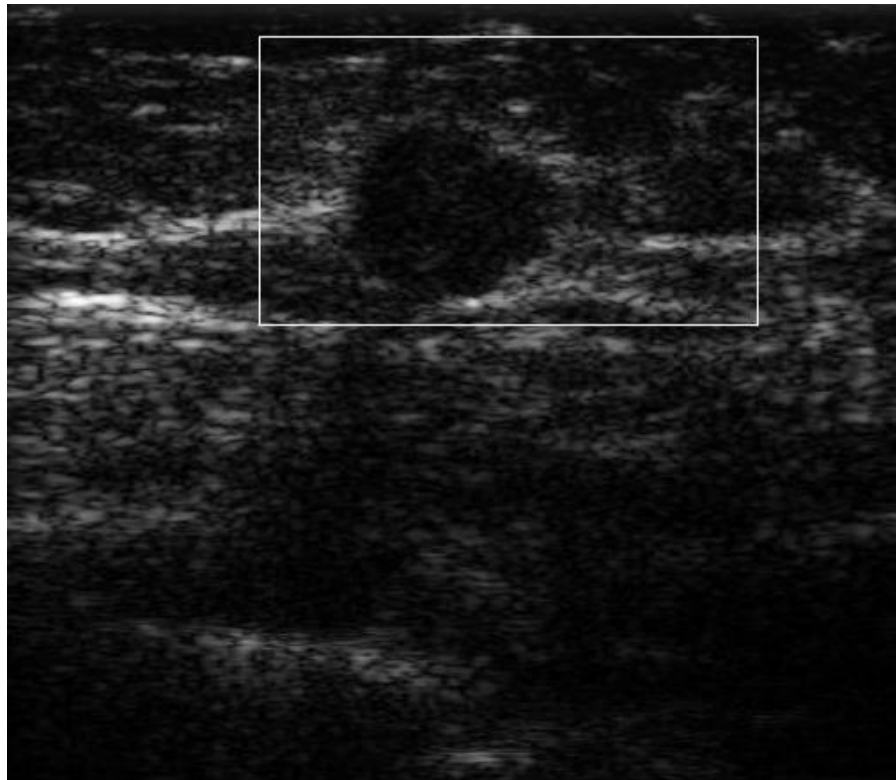


Figure 4.17 Rectangular ROI on the original image

Fig 4.18(a), 4.18(b), 4.18(c) and 4.18(d) shows four generated ROIs from our proposed algorithm.

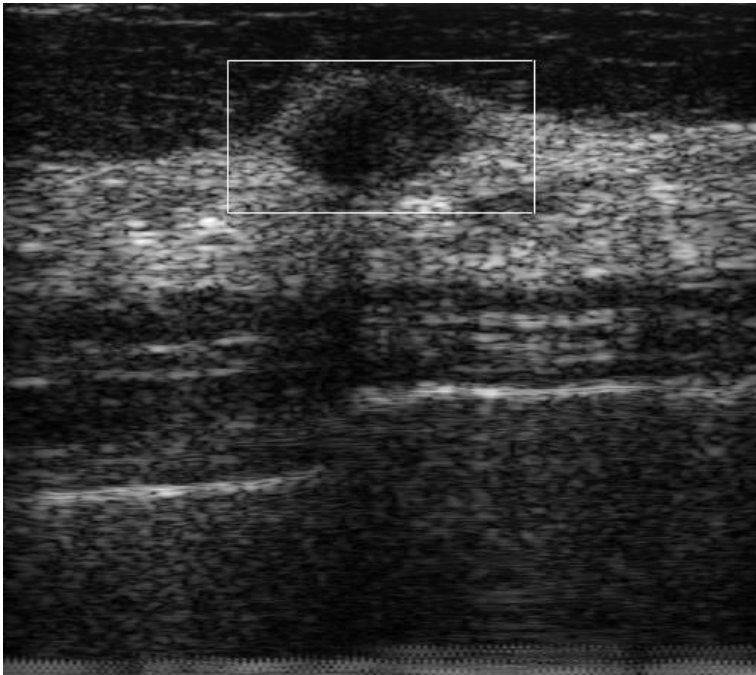


Figure 4.18 (a)

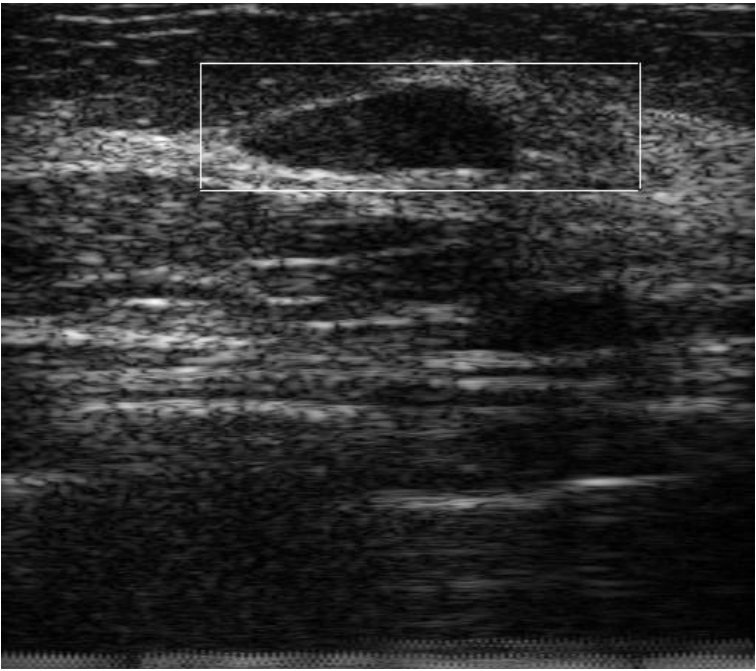


Figure 4.18 (b)

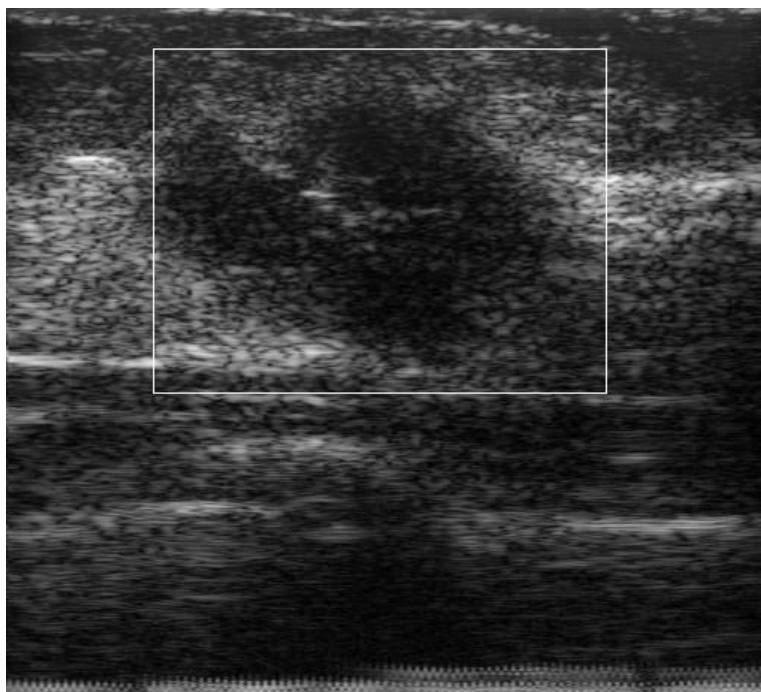


Figure 4.18 (c)

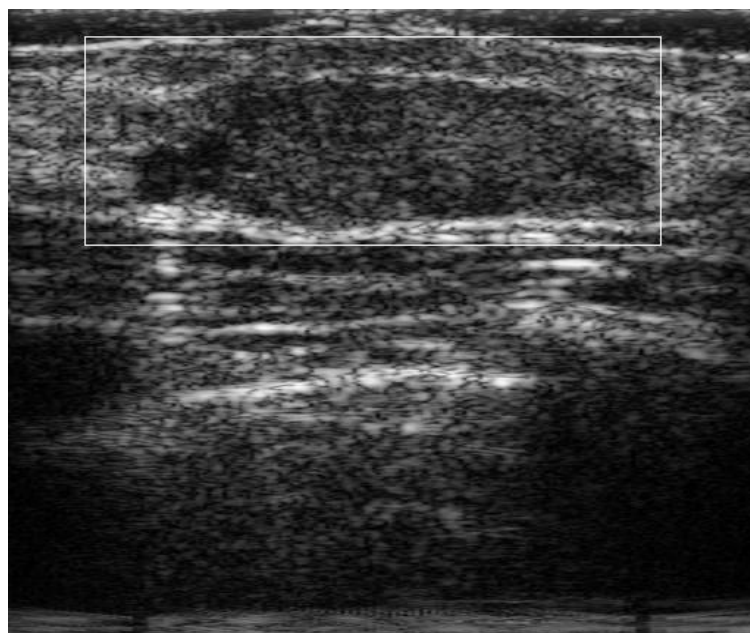


Figure 4.18 (d)

Figure 4.18 Successfully Generated ROIs

Chapter 5

Automatic Lesion Segmentation from the derived ROI image

5.1 Introduction

Automatic lesion segmentation is a crucial step in achieving full automation in CAD systems. A fully automatic CAD can minimize the effect of the operator-dependent nature inherent in ultrasound imaging [71] and make the diagnosis process reproducible [31]. It is quite important to be accurate in segmentation because many crucial features for discriminating benign and malignant lesions are based on the contour, shape, volume and texture of the segmented lesion which further runs through classifier for final decision. So it is very much crucial to never lose any important image feature in the segmentation phase. Therefore, an accurate segmentation enhances the probability of achieving correct diagnosis.

However, there are characteristic artifacts, such as attenuation, speckle, shadows, and signal dropout, which make the segmentation task complicated; these artifacts are due to the orientation dependence of acquisition that can

result in missing boundaries [31]. These artifacts makes BUS image segmentation task a complicated and challenging one.

In this section, we achieve segmentation in two methods which are discussed below in details.

5.2 Method 01

This method includes six steps. These are shown in the Fig 5.1.

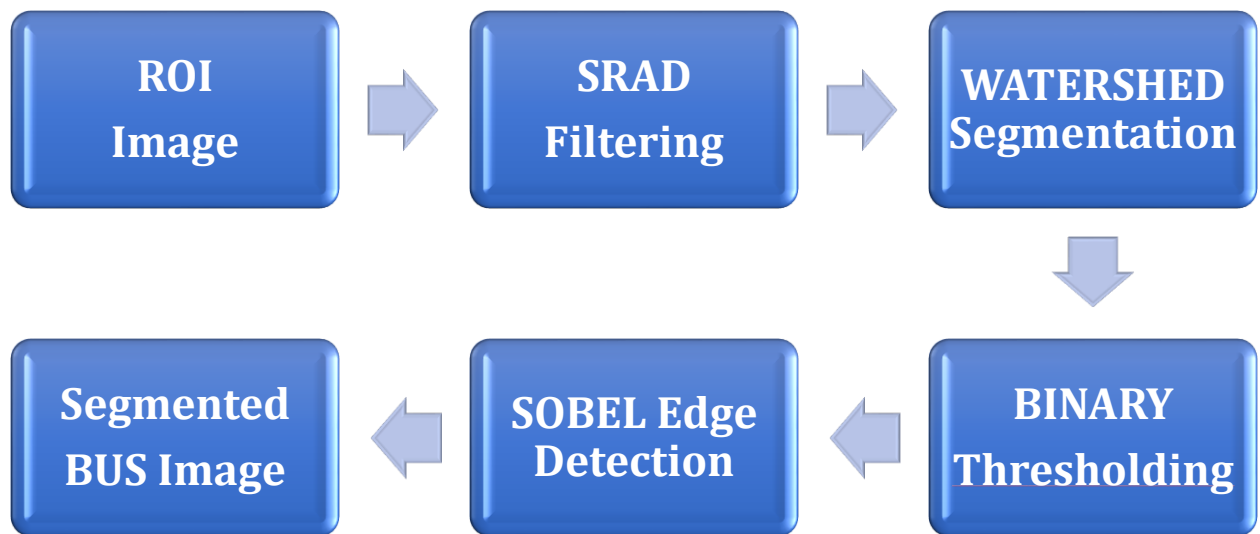


Figure 5.1 Proposed Method 01

Step 01: Getting the ROI Image

First of all, we input the ROI image extracted from the method mentioned in chapter 3 and starts processing on it to achieve better accuracy and to avoid unwanted segmentation as ROI generation phase already removes unwanted tissues, muscles, fats etc. from the original image.

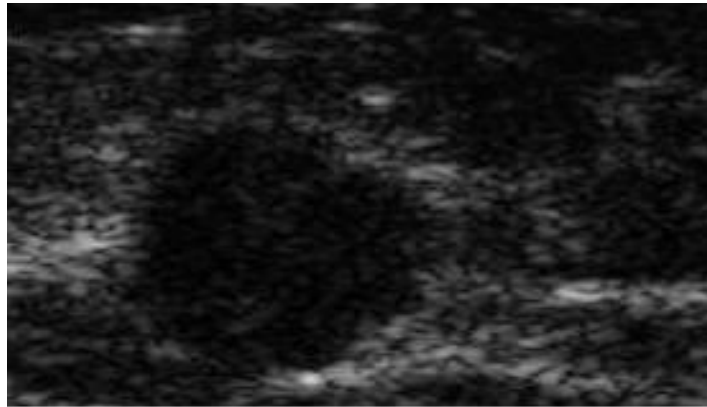


Figure 5.2 ROI Image

Step 02: Speckle Reducing Anisotropic Diffusion (SRAD) Filtering

SPECKLE, a form of multiplicative, locally correlated noise which arises from coherent wave interference [72] and gives a granular appearance to an otherwise homogeneous region of tissue. Ultrasonic produced by ultrasonic probe is reflected by the body internal and external interface and returned the probe. A series of coherent scattering of waves are induced due to the signal of the probe random fluctuating. Thus speckle noise occurs with this random fluctuating in medical ultrasound imaging system. Speckle reduces image contrast and detail resolution, and makes it difficult to identify abnormal tissue patterns (or texture) that may indicate disease [73].

Speckle noise can be mathematically modelled as

$$f(x, y) = g(x, y) \cdot \eta_m(x, y) + \eta_a(x, y) \quad 5.1$$

In this equation 5.1

$g(x, y)$ = Real Noisy image

$g(x, y)$ = Original Image

$\eta_m(x, y)$ = Multiplicative Noise Function

$\eta_a(x, y)$ = Additive Noise Function

Compared to additive noise, multiplicative noise is signal dependent and is difficult to be removed without impairing image details [74]. Since additive noise is considered to be lower than multiplicative noise, [75] proposed the following signal dependent noise model for speckle specification in ultrasound images:

$$f(x, y) = g(x, y) \cdot \eta_m(x, y) \tag{5.2}$$

In BUS image, it is very much crucial to preserve the edges and at the same time reduce speckle noise as much as possible. For achieving this purpose, we used SRAD filtering technique. The following features of SRAD filtering makes it superior over other adaptive de-speckle filtering techniques such as Lee and Kuan filter, Frost filter etc. [76]:

- A partial differential equation (PDE) approach to speckle removal;
- Allows the generation of an image scale space (a set of filtered images that vary from fine to coarse) without bias due to filter window size and shape;
- SRAD not only preserves edges but also enhances edges by inhibiting diffusion across edges and allowing diffusion on either side of the edge;
- SRAD is adaptive and does not utilize hard thresholds to alter performance in homogeneous regions or in regions near edges and small features.

Basic Theory behind SRAD Filtering

Given an intensity image $I_o(x, y)$ having finite power and no zero values over the image support Ω , the output image $I(x, y; t)$ is evolved according to the following PDE [76]:

$$\frac{\partial I(x, y; t)}{\partial t} = \text{div}[c(q)\nabla I(x, y; t)]$$

$$I(x, y; 0) = I_o(x, y), \left(\frac{\partial I(x, y; t)}{\partial \vec{n}} \right) \Big|_{\partial\Omega=0} \quad 5.3$$

In the equation 5.3

$\partial\Omega$ = Border of Ω

\vec{n} = Outer normal to $\partial\Omega$

The diffusion coefficient is determined by:

$$c(q) = \frac{1}{1 + \frac{[q^2(x, y; t) - q_0^2(t)]}{[q_0^2(t)(1 + q_0^2(t))]} \quad 5.4$$

And the instantaneous coefficient is given by:

$$q(x, y; t) = \sqrt{\frac{1/2(|\nabla I|/I)^2 - (1/4^2)(|\nabla^2 I|/I)^2}{[1 + (1/4)(\nabla^2 I/I)]^2}} \quad 5.5$$

The initialized $q_0(t)$ is given by

$$q_0(t) = \frac{\sqrt{[\text{var } z(t)]}}{z(t)} \quad 5.6$$

Here, $z(t)$ is the most homogenous region in t

Implementing the equations (5.3-5.6), we applied SRAD filtering on our ROI image and got out SRAD filtered image shown in Fig 5.4

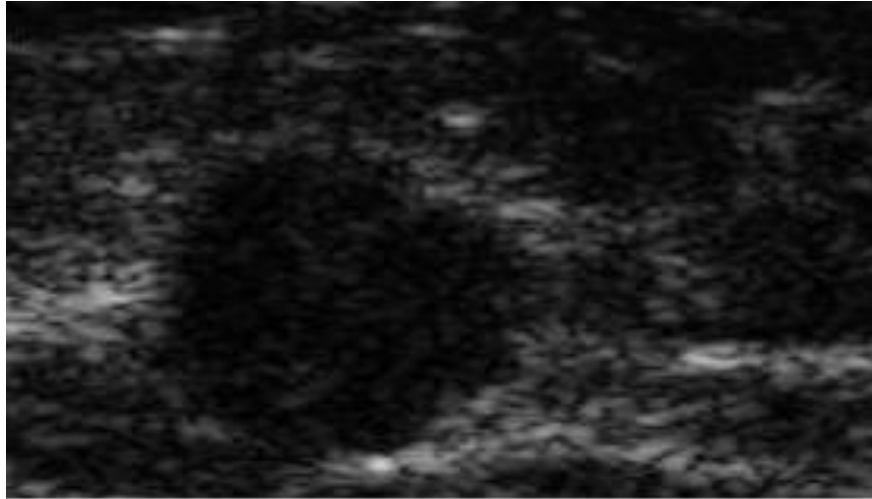


Figure 5.3 ROI Image before filtering

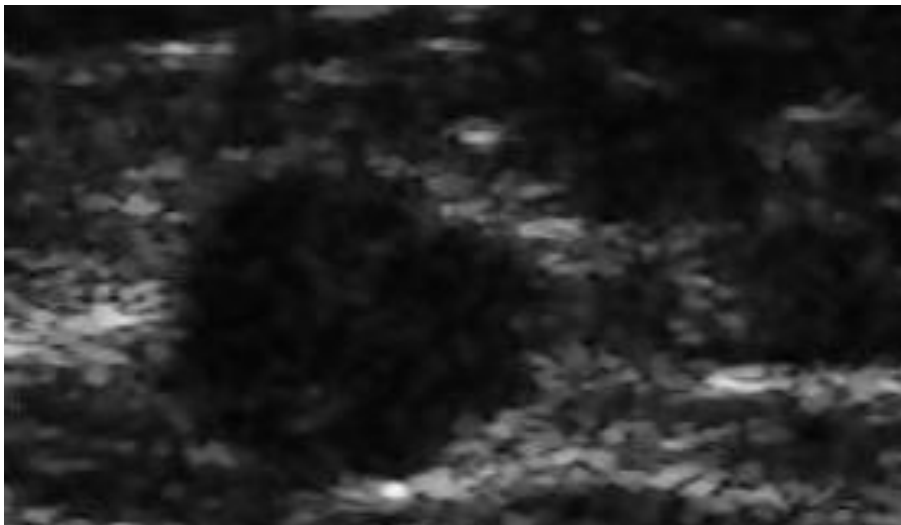


Figure 5.4 ROI Image after SRAD filtering

Step 03: Watershed Segmentation

Basic Concept

The basic concept of watershed is based on visualizing a gray level image into its topographic representation, which includes three basic notions: minima, catchment basins and watershed lines. In the image of Fig.5.6, if we imagine the bright areas have "high" altitudes and dark areas have "low" altitudes, then it might look like the topographic surface illustrated by Fig. 5.5. In this surface, it is natural to consider three types of points:

- (1) Points belonging to the different minima;
- (2) Points at which water would fall with certainty to a single minimum;
- (3) Points at which water would be equally likely to fall to more than one minimum [77].

The first type of points forms different minima of the topographic surface. The second type points which construct a gradient interior region is called catchment basin.

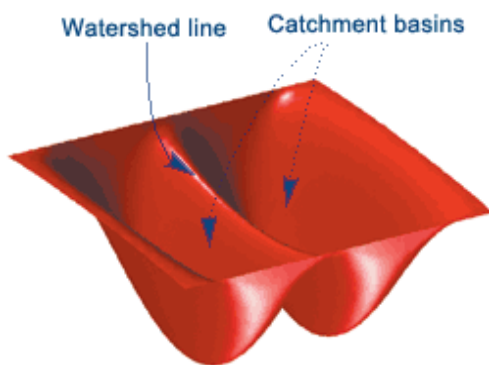


Figure 5.6 Topographic Relief Image

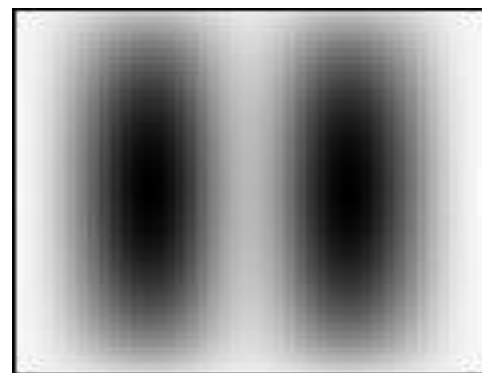


Figure 5.5 A Gray Scale Image

The algorithm introduced by Luc Vincent and Pierre Soille is based on the concept of “immersion”. Each local minima of a gray-scale image I which can be regarded as a surface has a hole and the surface is immersed out into water. Then, starting from the minima of lowest intensity value, the water will progressively fill up different catchment basins of image (surface) I . Conceptually, the algorithm then builds a dam to avoid a situation that the water coming from two or more different local minima would be merged. At the end of this immersion process, each local minimum is totally enclosed by dams corresponding to watersheds of image (surface). This flooding process is shown in Fig 5.7.

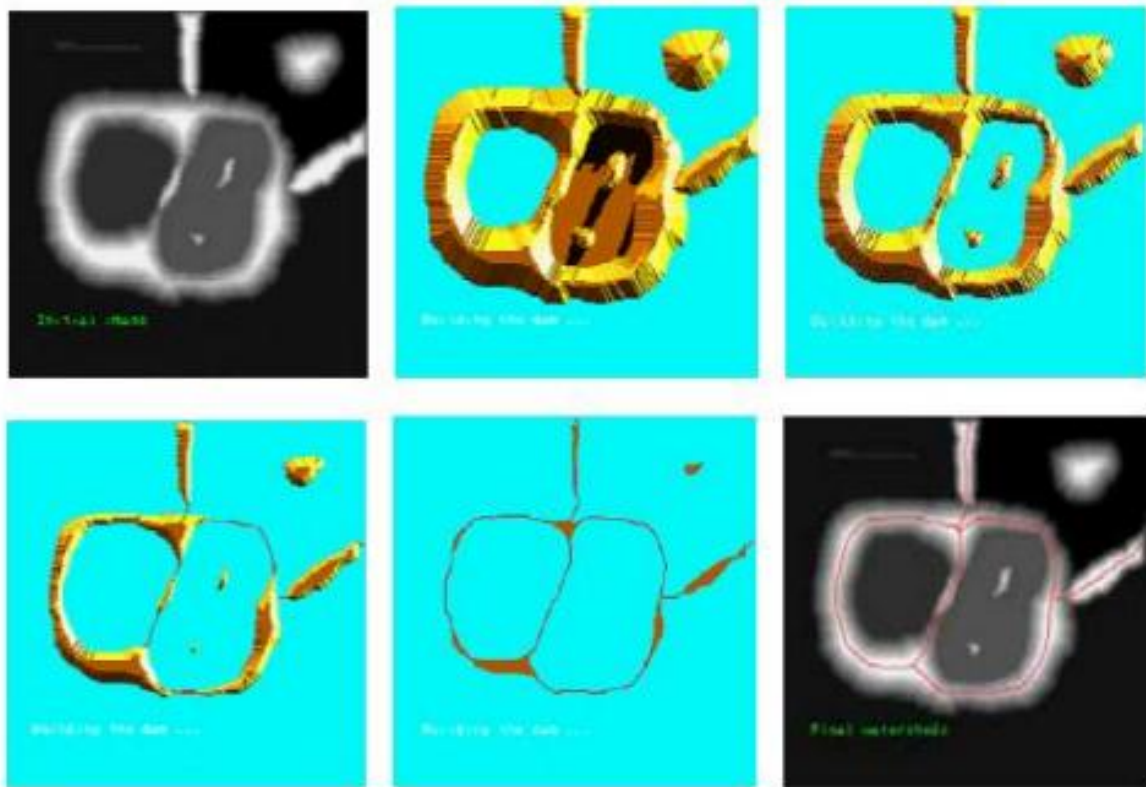


Figure 5.7 Flooding in Watershed Algorithm

Due to wide variation of intensity in the BUS image, the watershed segmentation suffers from over-segmentation of the image. To overcome this problem, we suppressed some local minimums in order to achieve our desired segmentation. Finally, we applied this algorithm on our SRAD filtered image. Fig 5.8 shows the gray scale watershed image and Fig 5.9 shows the color mapped watershed image.



Figure 5.8 Gray Scale Watershed Image

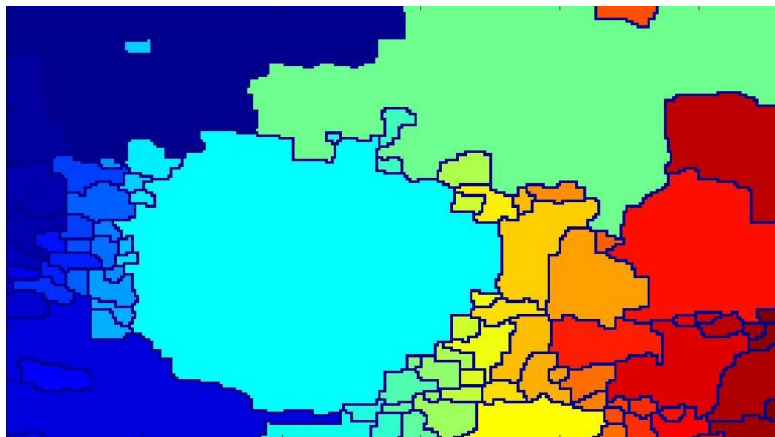


Figure 5.9 Color Mapped Watershed Image

Step 04: Binary Thresholding

We observed the large connected component of watershed image is our desired lesion. Therefore we followed the following principle to form the binary image:

- Ranked all the segmented region of the watershed image based on area
- Formed binary image by preserving the largest connected area in the watershed image

Thus we get a binary image having only our lesion. Fig 5.10 shows the binary image.

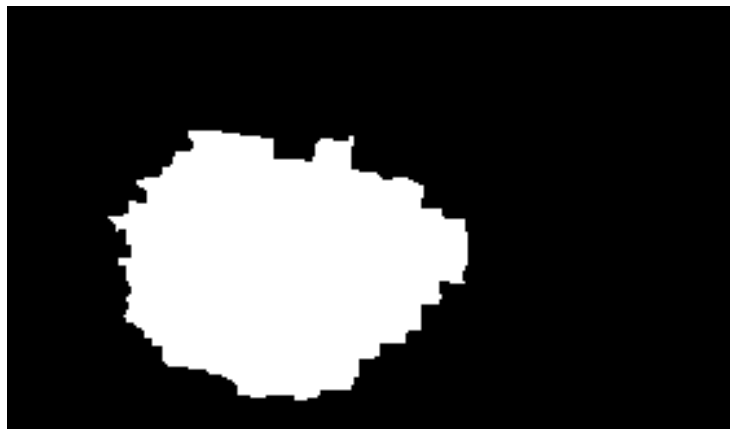


Figure 5.10 Binary Image

Step 05: SOBEL Edge Detection

In this step we apply the SOBEL edge detection method.

Fig 5.11 shows a 3x3 neighborhood of an image I with green colored box showing the center pixel on which the SOBEL edge detection will be applied. The steps of SOBEL edge detection are:

- It uses a 3x3 filter mask as shown in Fig 5.12 and Fig 5.13 to calculate gradient in every pixel location of the input image
- It returns edges at those points where the gradient of I is maximum

Z1	Z2	Z3
Z4	Z5	Z6
Z7	Z8	Z9

Figure 5.11 3x3 Image Neighborhood

-1	-2	-1
0	0	0
1	2	1

Figure 5.12 SOBEL Operator for x direction

-1	0	1
-2	0	2
-1	0	1

Figure 5.13 SOBEL Operator for y direction

Therefore the gradient equation becomes:

$$g_x = \frac{\partial I}{\partial x} = (z_7 + 2z_8 + z_9) - (z_1 + 2z_2 + z_3) \quad 5.7$$

$$g_y = \frac{\partial I}{\partial y} = (z_3 + 2z_6 + z_9) - (z_1 + 2z_4 + z_7) \quad 5.8$$

Applying this SOBEL Edge detector on our binary image, we get the edge of our lesion as shown in Fig 5.14.

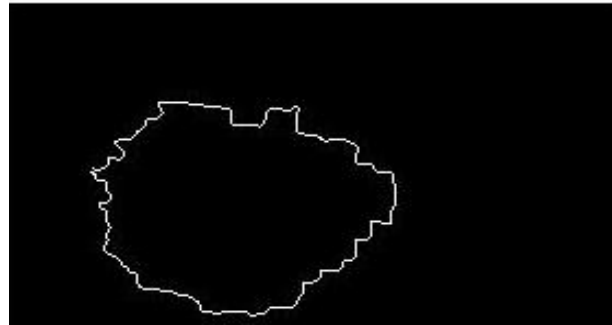


Figure 5.14 SOBEL Edge Detection

Step 06: Segmented Image

Finally we superimpose our detected edge on the original image and get our desired automatic segmentation. Fig 5.15 shows the final segmented image.

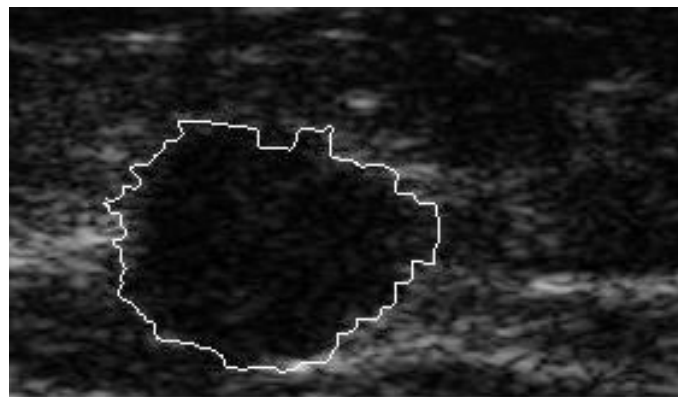


Figure 5.15 Segmented Image

5.3 Method 02

In the method 02, we made modifications in step 03. Instead of applying watershed segmentation we applied entropy filtering in step 03. Fig 5.16 shows the steps in method 02.

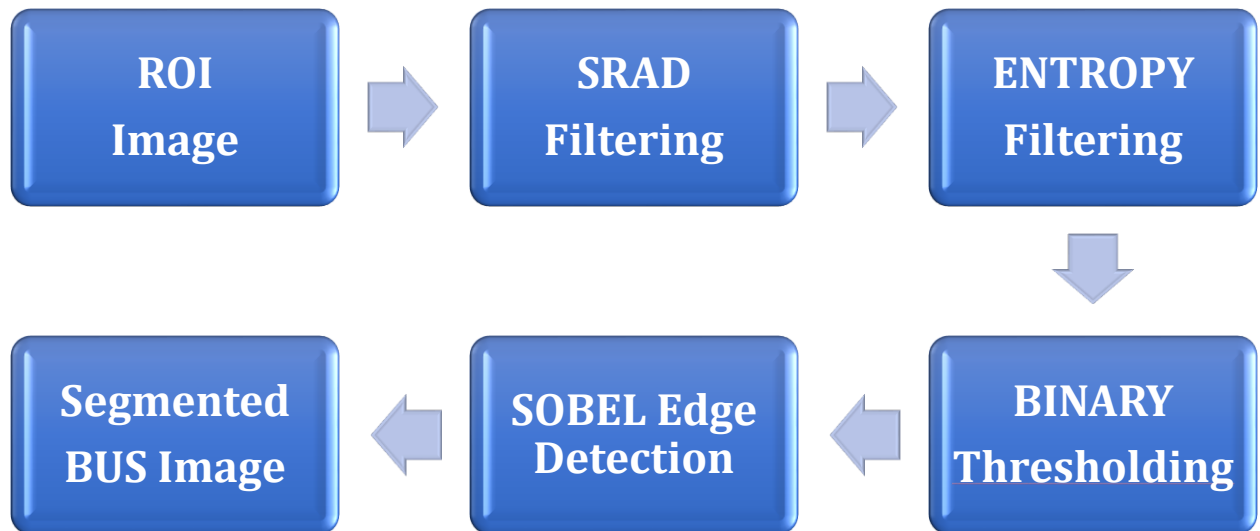


Figure 5.16 Proposed Method 02

Modified Steps

Step 03: Entropy Filtering

In this step we applied entropy filtering on SRAD filtering image. Fig 5.17 shows our entropy filtered image.

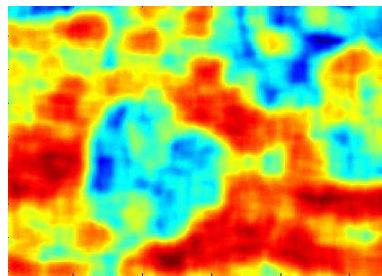


Figure 5.17 Entropy Filtering

Step 04: Binary Thresholding and Ranking

We transformed our entropy filtered image into binary image using entropy thresholding. For our thresholding, we used following equation for threshold determination:

$$EnTh = \frac{MaximumEntropy + MinimumEntropy}{2} \quad 5.9$$

After thresholding, we ranked the rest region to get the final lesion. Fig 5.18 shows binary image after thresholding and Fig 4.19 shows the image with the lesion.



Figure 5.18 Binary Image



Figure 5.19 Binary Image with the winning region

Step 05: SOBEL Edge Detection

Then we applied SOBEL Edge detection to detect the edge from the binary image. Fig 5.20 shows the detected edge.



Figure 5.20 Detected Edge

Step 06: Segmented Image

Finally we superimpose our detected edge on the original image and get our desired automatic segmentation. Fig 5.21 shows the final segmented image.

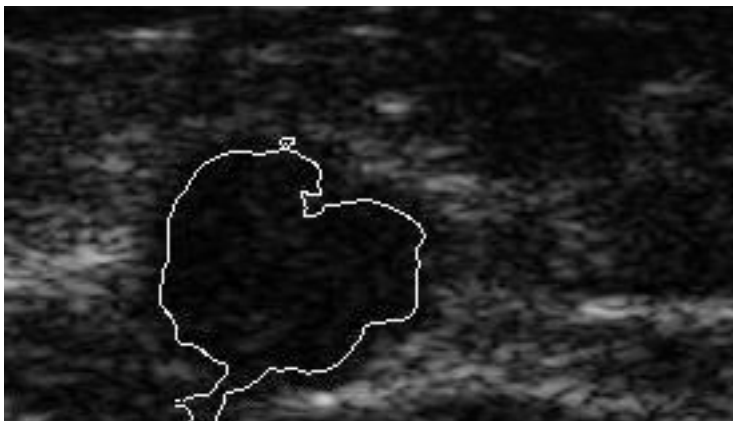


Figure 5.21 Segmented Image

5.4 Segmentation Results

5.4.1 Results from Method 01

Fig 5.22(a), 5.22(c) and 5.22(c) shows the segmented images using method 01.

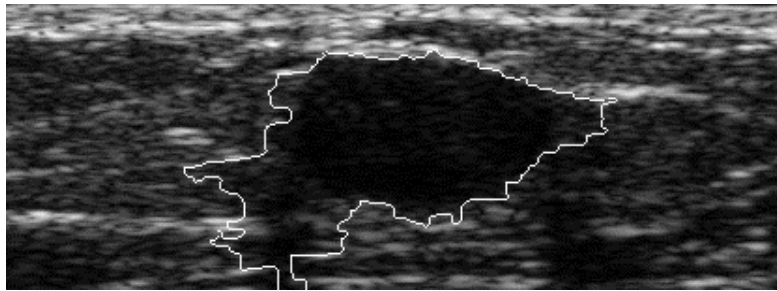


Figure 5.22 (a)

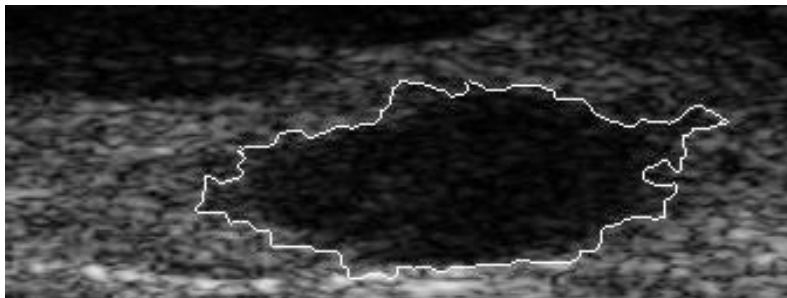


Figure 5.22 (b)

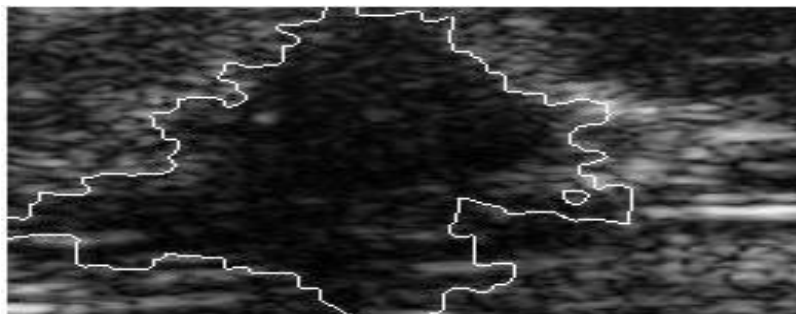


Figure 5.22 (c)

Figure 5.22 Segmented images using method 01

5.4.2 Results from Method 02

Fig 5.23(a), 5.23(c) and 5.23(c) shows the segmented images using method 02.

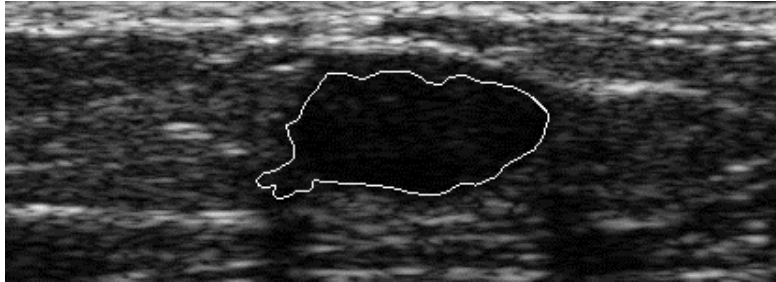


Figure 5.23 (a)

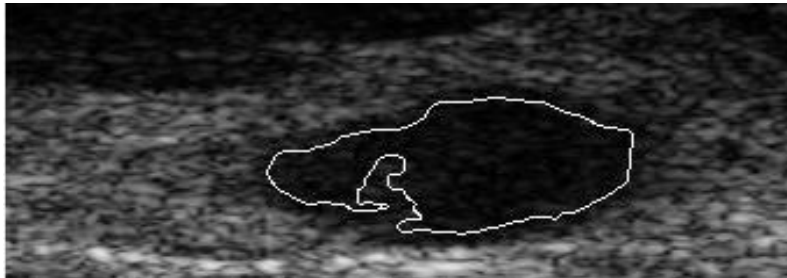


Figure 5.23 (b)

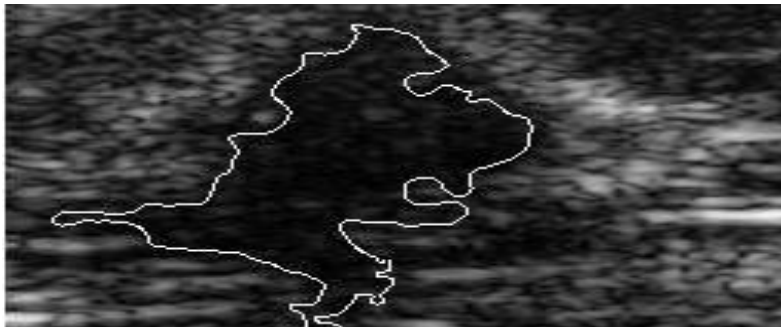


Figure 5.23 (c)

Figure 5.23 Segmented images using method 02

Chapter 6

Quantitative Evaluation of Segmentation Results

In this section, we try to validate our proposed algorithm by comparing our segmented image with the manually delineated ground truth image. We evaluate the performance of our method using four statistical metrics as follows:

- Dice Over Lap Coefficient (DOC)
- Jaccard Coefficient (JC)
- True Positive (TP) Area Ratio
- False Positive (TP) Area Ratio
- Hausdorff distance (HD)

6.1 Area Error Metrics

Area error metrics can evaluate how much of the lesion region is correctly covered by the generated lesion region and how much is wrongly covered.

The metrics used to evaluate this error are:

$$\text{a) TP Area Ratio [7]} = \frac{|A_m \cap A_a|}{|A_m|}$$

$$\text{b) FP Area Ratio [7]} = 1 - \frac{|A_m \cap A_a|}{|A_m|}$$

$$\text{c) Similarity or Jaccard Coefficient [17]} = \frac{|A_m \cap A_a|}{|A_m \cup A_a|}$$

$$\text{d) Dice Overlap Coefficient} = \frac{|A_m \cap A_a|}{|A_m| + |A_a|}$$

Following Fig 6.1 depicts the area error evaluation process.

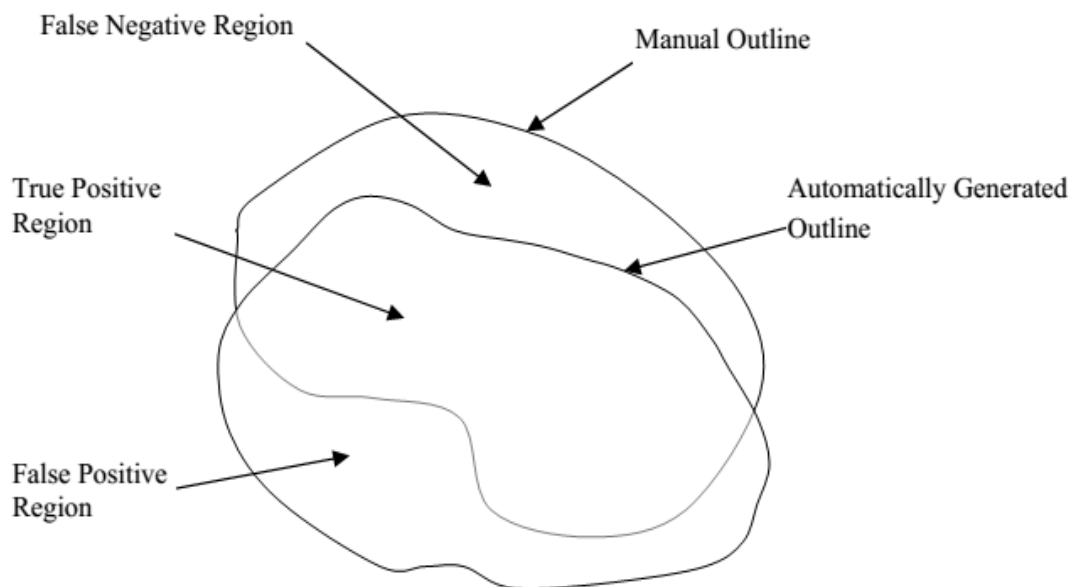


Figure 6.1 Areas corresponding to TP, FP, and FN regions

6.2 Boundary Error Metrics

We use boundary error metrics to analyze the difference between the contours generated by the proposed method and the contours marked by the radiologist. In our case we have used Hausdorff distance (HD) [7] which measures the worst possible disagreement between two contours.

Let us denote the manually delineated boundary as $Q = \{q_1, q_2, \dots, q_\gamma\}$ and the computer segmented result as $P = \{p_1, p_2, \dots, p_\mu\}$ and each element of Q or P is a point on the corresponding contour. We find the distances of every point in P to all points in Q, and define the shortest distance of p_j to contour Q as:

$\forall p_j \in P, j = 1, \dots, \mu$, we find

$$d(p_j, Q) = \min_w \|p_j - q_w\|, w = 1, \dots, \gamma$$

where $\| * \|$ is 2D Euclidian Distance.

Now HD is defined as:

$$HD = \max_j d(p_j, Q), j = 1, \dots, \mu$$

6.3 Materials

- Total 30 breast ultrasound images are used for analysis
- Out them, 23 images yielded correct results for ROI detection and 15 images were segmented

Case 01

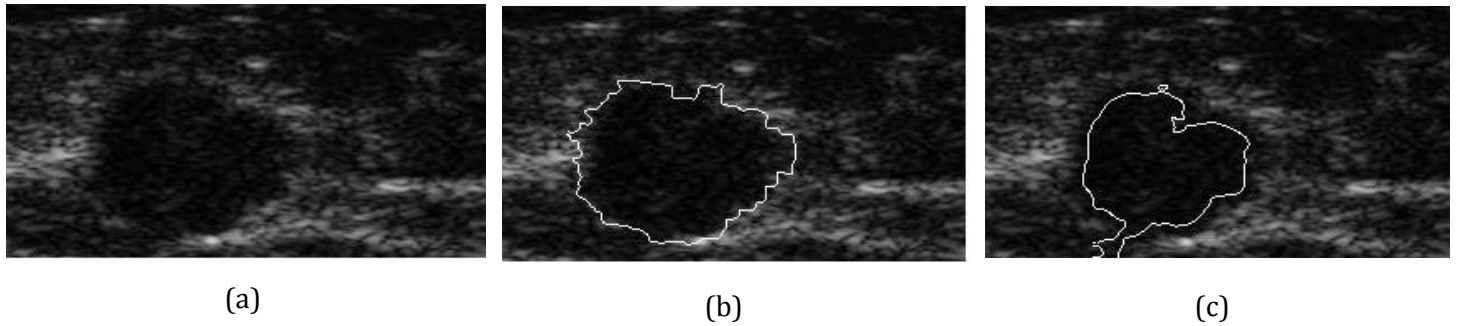


Figure 6.2 Case 01: (a) ROI image, (b) Watershed image, (c) Entropy image

Table 6.1 Comparison between two proposed methods for case 01

Metrics	Watershed Method	Entropy Method
TP Area Ratio	0.9634	0.6588
FP Area Ratio	0.0366	0.3416
JC	0.8715	0.6449
DOC	0.9314	0.7841
HD	1.5764	2.0116

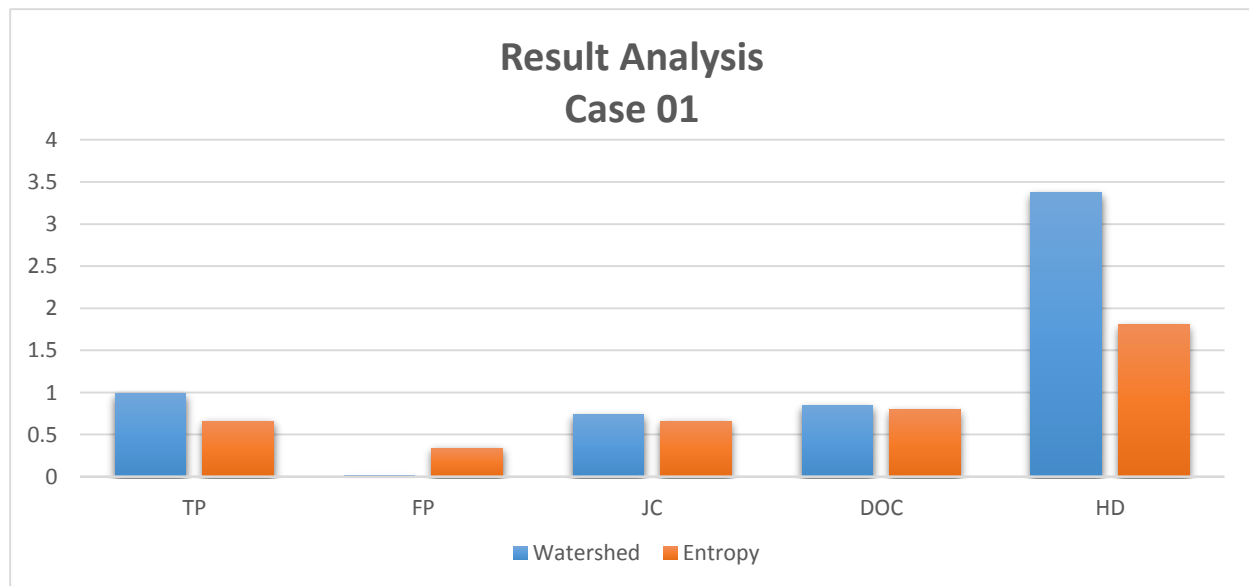


Figure 6.3 Result comparison for case 01

Case 02

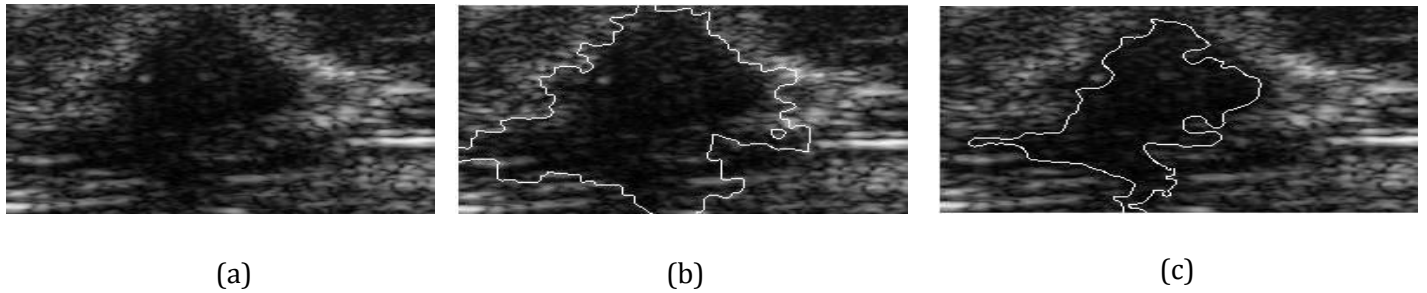


Figure 6.4 Case 02: (a) ROI image, (b) Watershed image, (c) Entropy image

Table 6.2 Comparison between two proposed methods for case 02

Metrics	Watershed Method	Entropy Method
TP Area Ratio	0.9780	0.7500
FP Area Ratio	0.0220	0.2500
JC	0.5880	0.7092
DOC	0.7405	0.8299
HD	4.5214	2.3359

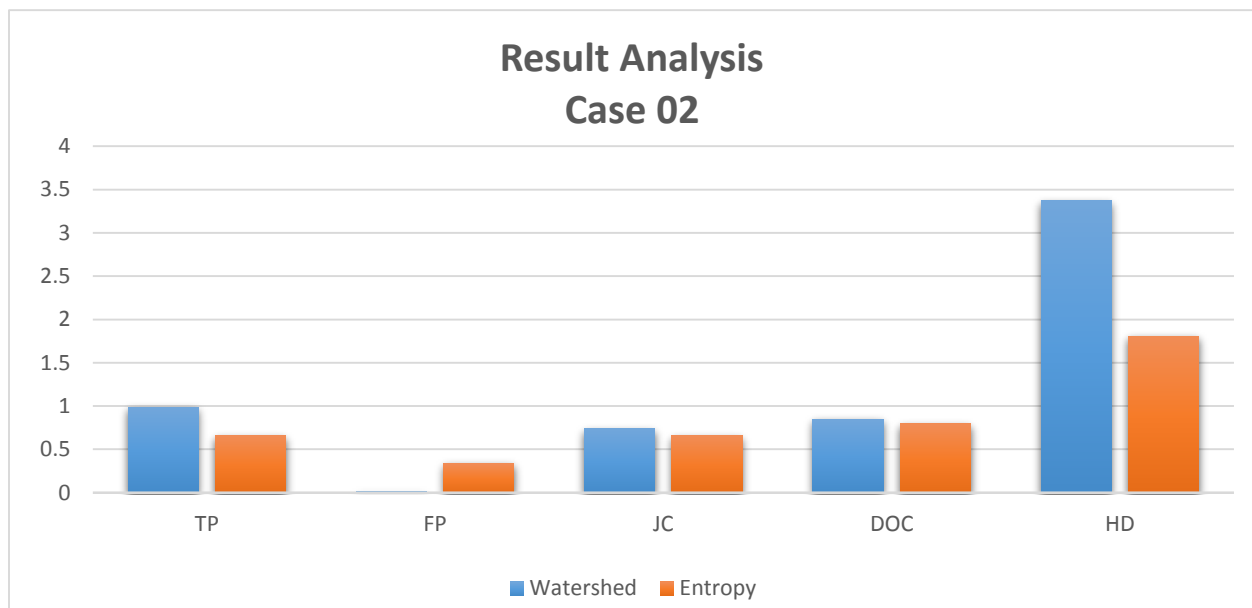


Figure 6.5 Result comparison for case 02

Case 03

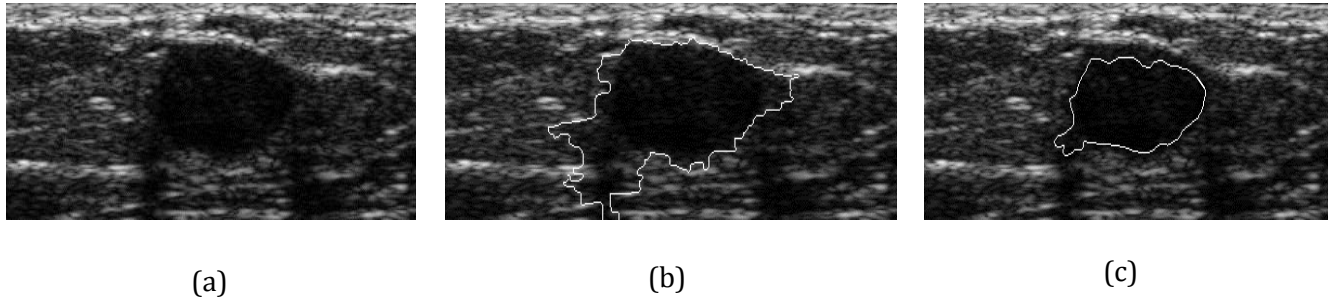


Figure 6.6 Case 03: (a) ROI image, (b) Watershed image, (c) Entropy image

Table 6.3 Comparison between two proposed methods for case 03

Metrics	Watershed Method	Entropy Method
TP Area Ratio	0.9868	0.6621
FP Area Ratio	0.0132	0.3379
JC	0.7377	0.6605
DOC	0.8490	0.7955
HD	3.3725	1.8061

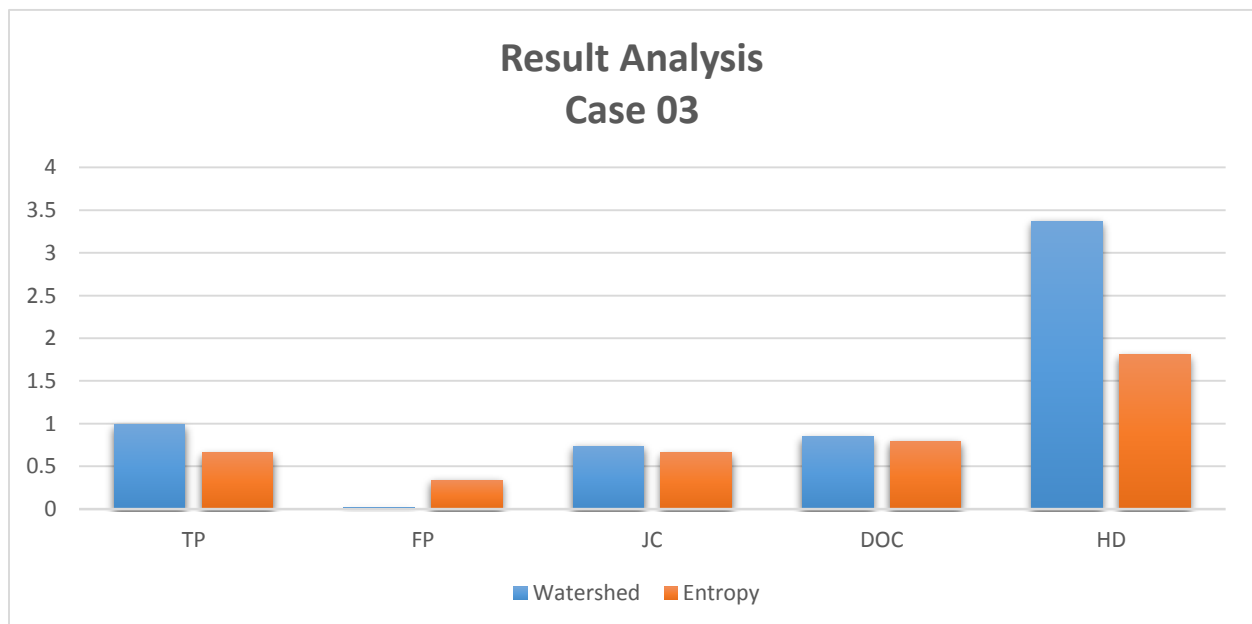


Figure 6.7 Result comparison for case 03

6.4 Result Analysis

From analyzing the results, we observe that in most of the case watershed method yielded better result than the entropy based method. But still watershed encompasses larger area around the lesion while entropy misses the region by encompassing smaller area. So possible improvement of the algorithm may be an edge derived from averaging the resultants from both methods.

Chapter 7

Future Development and Conclusion

In this thesis, we came up a segmentation algorithm which is capable of automatically generate ROI accurately. The whole system consisted of two major steps:

- Automatic ROI Generation
- Automatic Lesion Segmentation from the ROI image

The whole system overview is given in Fig 7.1

Though our system successfully generates ROI image in most of the case, but still it suffers from some limitations. These are:

- a) Too much speckle corrupted image provides anomalous entropy value which results in wrong ROI detection;
- b) The accuracy of ROI detection is a direct function of shadowing artifacts of the image thus too much shadowing results in erroneous detection;
- c) Too much speckle results in false radius in ROI detection phase;
- d) In segmentation stage, sometimes watershed method encompasses larger area while entropy method encompasses smaller area which is a hindrance in persevering correct shape of the segmented lesion.

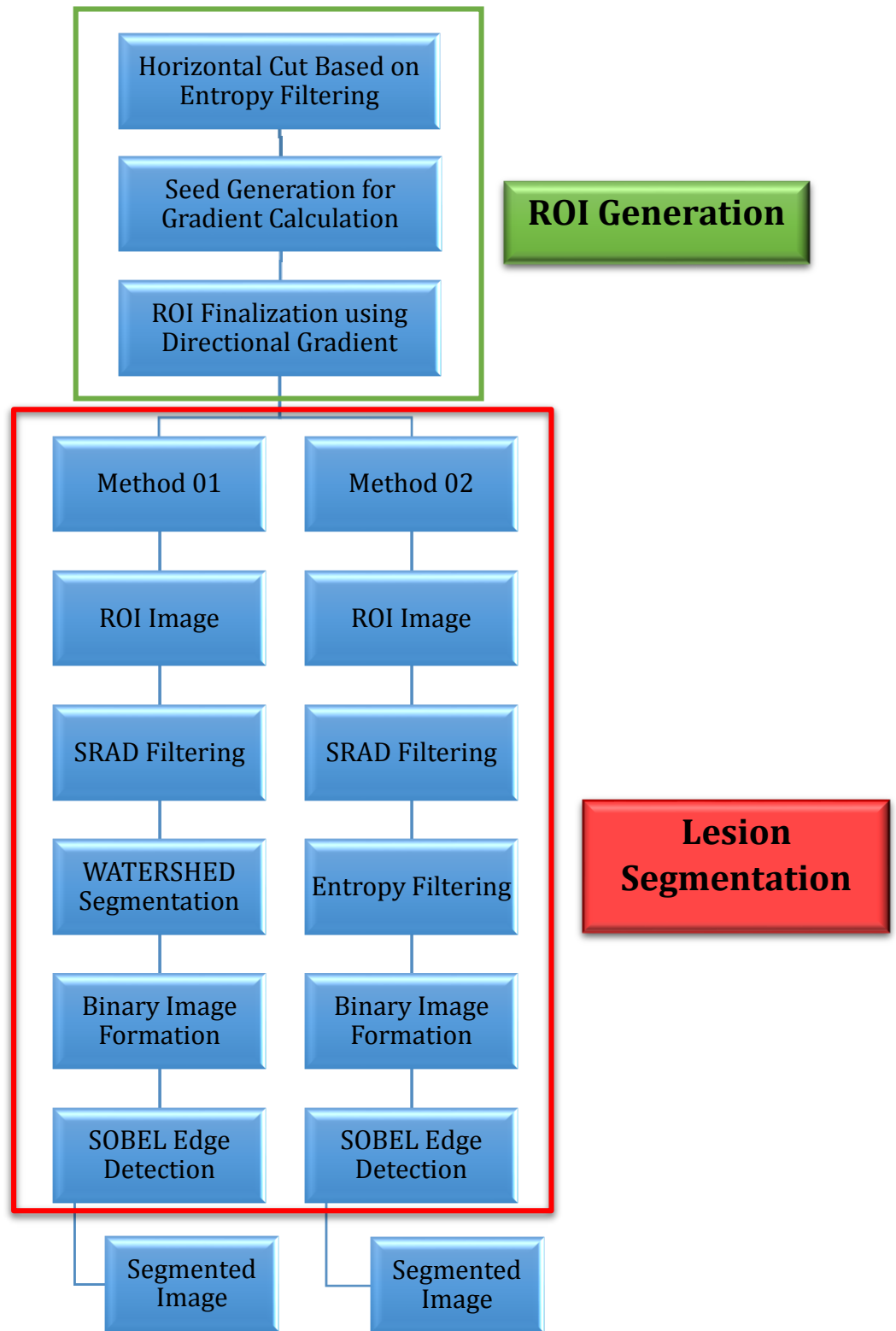


Figure 7.1 Whole system overview of proposed methods

Potential Future works may listed as follows:

- a) Solving the problems in ROI detection phase;
- b) Mathematical modelling of Shadowing Artifact of BUS image;
- c) Improving Automatic Segmentation of detected ROI image by creating an edge which is the average of the edge achieved from watershed method and entropy method.

Bibliography

- [1] Garcia, M., Jemal, A., Ward, E., Center, M., Hao, Y., Siegel, R., and Thun, M. *Global Cancer Facts & Figures 2007*, American Cancer Society, 2007.
- [2] American Cancer Society, *Cancer Facts & Figures 2008*, American Cancer Society, 2008.
- [3] American Cancer Society, *Cancer Facts & Figures 2009*, American Cancer Society, 2009.
- [4] American Cancer Society, *Breast Cancer Facts & Figures 2007-2008*, American Cancer Society, 2008.
- [5] Network of Strength. *Breast Cancer Statistics*. 2009.
<http://www.networkofstrength.org/information/bcnews/stats.php>. Jan. 2010.
- [6] Cheng, H.D., Cai, X., Chen, X., Hu, L., and Lou, X. Computer-aided detection and classification of micro calcifications in mammograms: a survey. *Pattern Recognition* 36,12 (2003), 2967-2991.
- [7] American Cancer Society. *What Are the Key Statistics for Breast Cancer?* 2009.
http://www.cancer.org/docroot/cric/content/cric_2_4_1x_what_are_the_key_statistics_for_breast_cancer_5.asp. Jan. 2010.
- [8] Committee on Technologies for the Early Detection of Breast Cancer, *Mammography and Beyond: Developing Technologies for the Early Detection of Breast Cancer*, S.J. Nass, I.C. Henderson, and J.C. Lashof, Eds. National Cancer Policy Board, Institute of Medicine, and Commission on Life Studies, National Research Council, 2001.
- [9] Xu Liu, Zhimin Huo and Jiwu Zhang. Automated segmentation of breast lesions in ultrasound images. *Proceedings of the 2005 IEEE Engineering in Medicine and Biology, 27th Annual Conference Shanghai, China, September 1-4, 2005*.
- [10] E. J. Bond, X. Li, S. C. Hagness, B.D. Van Veen, "Microwave Imaging via Space-Time Beamforming for Early Detection of Breast Cancer", *IEEE Trans. Ant. Propag.*, vol. 51, no. 8, Aug. 2003.
- [11] X. Li and S.C. Hagness, "A confocal microwave imaging algorithm for breast cancer detection," *IEEE Microwave Wireless Components Lett.*, vol. 11, pp. 130-32, Mar. 2001.
- [12] S.C. Hagness, A. Taflove, and J.E. Bridges, "Two-dimensional FDTD analysis of a pulsed microwave confocal system for breast cancer detection: fixed-focus and antenna-array sensors", *IEEE Trans. Biomed. Eng.*, vol. 45, pp. 1470-1479, Dec. 1998.
- [13] O. Husby and H. Rue, "Estimating blood vessel areas in ultrasound images using a deformable template model," *Statist. Model.*, vol. 4, no.3, pp. 211-226, 2004.
- [14] Daxi Wang, Yuan Fang, Bo Hu, Hanqiang Cao, "B-scan Image feature Extraction of fatty liver" 2012 IEEE sixth international conference on internet computing for science and engineering.
- [15] Mitsuhiro and Akira Taguchi, "The learning type of hybrid median filters," *IEEE Transactions* 1997.
- [16] HPrasana Kumar and S Srinivasan, "performance analysis of filters for speckle reduction in medical polycystic ovary ultrasound images." *ICCCNT 2012*.

- [17] R.Sivakumar,M.K.Gayathri and D.Neduraman, “speckle filtering of ultrasound B-Scan images a comparative study between spatial and diffusion filters, IEEE Conference on open systems (ICOS 2010),December 2010.
- [18] TaoHue, YaunyuanWang,YiGuo, “Despeckling ultrasound images based on blind deconvolution and maximum likelihood”, 2010 IEEE Transactions.
- [19] J.S.Lee, “Digital image enhancement and noise filtering by use of local statistics”, IEEE transactions, Mar 1980.
- [20] J.Saranya and S.Malarkhodi , “filtering and segmentation of a uterine fibroid with an ultrasound images, ”Proceedings of the international conference on pattern recognition, informatics and medical engineering (PRIME) , IEEE Mar. 2012.
- [21] A.Lopes, R.Touzi, and E.Nezry, “Adaptive speckle filters and scene heterogeneity” IEEETransactions, Nov 1990.
- [22] Sean Finn, MartinGalvin, Edward Jones, “Echocardiographic Speckle Reduction Comparison,”IEEE Transactions on ultrasonics, ferroelectronics and frequency control, January 2011.
- [23] Yu Deng, Hu Huang, “Ultrasound Image Segmentation Based On Anisotropic Diffusion Filtering,” IEEE transactions, 2010.
- [24] Mandeepsingh, Dr. Sukhwindersingh,Dr. SavitaKansal, “comparative analysis of spatial filters for speckle reduction in ultrasound images” IEEE Transactions,2009.
- [25] S.Aja-Fernandez and C.Alberola Lopez, “On the estimation of the co-efficient of variation for anisotropic diffusion speckle filtering“ IEEE Trans. Image processing , nov 2002.
- [26] T.Crimmins, “Geometric filter for speckle reduction,”Appl.Opt.,vol24,pp1438-1443,1985.
- [27] L.J.Busse,T.R. Crimmins and J.R.Fienup, “A model based approach to improve the performance of geometric filter speckle reduction algorithm,” in IEEE Ultrason. Symp.,nov 1995.
- [28] Myungeun Lee, Yanjuan Chen, Soohyung Kim, Kwanggi Kim, 2011, Geometric Active Model for Lesion Segmentation on Breast Ultrasound Images.
- [29] Rafael Rodrigues, Ant´onio Pinheiro, Rui Braz, Manuela Pereira, J. Moutinho,2012,Towards Breast Ultrasound Image Segmentation using Multi-resolution Pixel Descriptors .
- [30] Moi Hoon Yap, Eran A. Edirisinghe, and Helmut E. Bez, 2008, A novel algorithm for initial lesion detection in ultrasound breast images.
- [31] Juan Shan,2011, A Fully Automatic Segmentation Method for Breast Ultrasound Images.
- [32] A.F.M. Kamal Uddin , Zohora Jameela Khan, Johirul Islam & Mahmud AM,2013, Cancer Care Scenario in Bangladesh.

- [33] Hasan A.H.M Nazmul, Uddin Md. Mostafa, Rafiquzzaman Md. Chowdhury, Sanchita Sharmin, Wahed Tania Binte, 2012, Distribution of Types of Cancers and Patterns of Cancer Treatment Among the Patients at Various Hospitals in Dhaka Division in Bangladesh .
- [34] M Halliwell, 2009, A tutorial on ultrasonic physics and imaging techniques.
- [35] A. Stavos, D. Thickman, C. Rapp, M. Dennis, S.Parker, and S. G. A., "Solid breast modules: Use of sonography to distinguish between benign and malignant lesions," *Radiology*, vol. 196, pp. 123–134, 1995.
- [36] V. Jackson, "Management of solid breast modules: What is the role of sonography?," *Radiology*, vol. 196, pp. 14–15, 1995.
- [37] P. Arger, C. Sehgal, E. Conant, J. Zuckerman, S. Rowling, and J. Patton, "Interreader variability and predictive value of is descriptions of solid masses: Pilot study," *Acad. Radiol.*, vol. 8, pp. 335–342, 2001.
- [38] Cobbold, Richard S. C. (2007). *Foundations of Biomedical Ultrasound*. Oxford University Press. pp. 422–423.
- [39] Merritt, CR (1 November 1989). "Ultrasound safety: what are the issues?". *Radiology* 173 (2): 304–306.
- [40] "Training in Diagnostic Ultrasound: essentials, principles and standards" (PDF). WHO. 1998. p. 2.
- [41] Stavros AT, Thickman D, Rapp CL et - al. Solid breast nodules: use of sonography to distinguish between benign and malign ant lesions. *Radiology*. 1995;196 (1): 123-34.
- [42] Rahbar G, Sie AC, Hansen GC et -al. Benign versus malignant solid breast masses: US differentiation. *Radiology*. 1999;213 (3): 889-94.
- [43] Cardeñosa G. *Clinical breast imaging, a patient focused teaching fi le*. Lippincott Williams & Wilkins. (2006).
- [44] Paredes ES. *Atlas of mammography*. Lippincott Williams & Wilkins. (2007).
- [45] Moi Hoon Yap, Eran A. Edirisinghe, and Helmut E. Bez, 2008, A novel algorithm for initial lesion detection in ultrasound breast images .
- [46] A. Madabhushi and D. N. Metaxas, "Combining low-, high-level and empirical domain knowledge for automated segmentation of ultrasonic breast lesions," *IEEE Trans. Med. Imag.*, vol. 22, no. 2, pp. 155–169, Feb. 2003.
- [47] K. Horsch, M. L. Giger, L. A. Venta, and C. J. Vyborny, "Automatic segmentation of breast lesions on ultrasound," *Med. Phys.*, vol. 28, no. 8, pp. 1652–1659, Aug. 2001.
- [48] K. Horsch, M. L. Giger, L. A. Venta, and C. J. Vyborny, "Computerized diagnosis of breast lesions on ultrasound," *Med. Phys.*, vol. 29, no. 2, pp. 157–164, Feb. 2002.
- [49] K. Horsch, M. L. Giger, C. J. Vyborny, and L. A. Venta, "Perfor-mance of computer-aided diagnosis in the interpretation of lesions on breast sonography," *Acad. Radiol.*, vol. 11, no. 3, pp. 272–280, Mar. 2004.

- [50] K. Drukker, M. L. Giger, K. Horsch, C. J. Kupinski, M. A. Vyborny, and E. B. Mendelson, "Computerized lesion detection on breast ultra-sound," *Med. Phys.*, vol. 29, no. 7, pp. 1438–1446, Jul. 2002.
- [51] D. R. Chen, R. F. Chang, W. J. Kuo, M. C. Chen, and Y. L. Huang, "Diagnosis of breast tumors with sonographic texture analysis using wavelet transform and neural networks," *Ultrasound Med. Biol.*, vol. 28, no. 10, pp. 1301–1310, Oct. 2002.
- [52] Y. L. Huang and D. R. Chen, "Watershed segmentation for breast tumor in 2-D sonography," *Ultrasound Med. Biol.*, vol. 30, no. 5, pp. 625–632, May 2004.
- [53] D. Boukerroui, A. Baskurt, J. A. Noble, and O. Basset, "Segmentation of ultrasound images—multiresolution 2-D and 3-D algorithm based on global and local statistics," *Pattern Recognit. Lett.*, vol. 24, no. 4–5, pp. 779–790, Feb. 2003.
- [54] G. F. Xiao, M. Brady, J. A. Noble, and Y. Y. Zhang, "Segmentation of ultrasound B-mode images with intensity inhomogeneity correction," *IEEE Trans. Med. Imag.*, vol. 21, no. 1, pp. 48–57, Jan. 2002.
- [55] Haralick, R. M., K. Shanmugam, and I. Dinstein, "Textural features for image classification," *IEEE Transactions on Systems, Man, and Cybernetics*, SMC-3, pp. 610–621, 1973.
- [56] Paredes ES. *Atlas of mammography*. Lippincott Williams & Wilkins. (2007).
- [57] Haralick, R.M., "Statistical and Structural Approaches to Texture," *Proceedings of the IEEE*, 67, pp. 786–804, 1979.
- [58] Zucker, S. W. and K. Kant, "Multiple -level Representations for Texture Discrimination," In *Proceedings of the IEEE Conference on Pattern Recognition and Image Processing*, pp. 609 -614, Dallas, TX, 1981.
- [59] D. R. Chen, R. F. Chang, W. J. Wu, W. K. Moon, and W. L. Wu, "3-D breast ultrasound segmentation using active contour model," *Ultrasound Med. Biol.*, vol. 29, no. 7, pp. 1017–1026, Jul. 2003.
- [60] R.-F. Chang, W.-J. Wu, W. K. Moon, W. M. Chen, W. Lee, and D.-R. Chen, "Segmentation of breast tumor in three-dimensional ultrasound images using three-dimensional discrete active contour model," *Ultra-sound Med. Biol.*, vol. 29, no. 11, pp. 1571–1581, Nov. 2003.
- [61] R.-F. Chang, W.-J. Wu, C.-C. Tseng, D.-R. Chen, and W. K. Moon, "3-D snake for ultrasound in margin evaluation for malignant breast tumor excision using mammotome," *IEEE Trans. Inf. Tech. Biomed.*, vol. 7, pp. 197–201, May 2003.
- [62] R.-F. Chang, W.-J. Wu, W. K. Moon, Y. H. Chou, and D.-R. Chen, "Support vector Machines for diagnosis of Breast tumors on ultrasound images," *Acad. Radiol.*, vol. 10, no. 2, pp. 189–197, 2003.
- [63] B. Sahiner, H. P. Chan, M. A. Roubidoux, M. A. Helvie, L. M. Hadjiiski, A. Ramachandran, C. Paramagul, G. L. LeCarpentier, A. Nees, and C. Blane, "Computerized characterization of breast masses on three dimensional ultrasound volumes," *Med. Phys.*, vol. 31, no. 4, pp. 744–754, Apr. 2004.

- [64] Boliu,H. D. Cheng, Jianhua Huang, Jiawei Tian, Jiafeng Liu, and Xianglong Tang, "Automated Segmentation Of Ultrasonic breast lesions using statistical texture classification and active contour based on probability distance".
- [65] Juanshan,H.D.Cheng, and Yuxuanwang , "Completely automated segmentation approach for breast ultrasound images using multiple-domain features" *Ultrasound in Med. & Biol.*, Vol. 38, No. 2, pp. 262–275, 2012.
- [66] Yanni Su, Yuanyuan Wang and Yi Guo , "Automatic Detection and Classification of Breast Tumors in Ultrasonic Images Using Texture and Morphological Features" *Open Med Inform J.* 2011; 5:26-37.
- [67] T Pun, "Entropic thresholding, a new approach" *Computer Graphics and Image Processing* Volume 16, Issue 3, July 1981, Pages 210–239.
- [68] Minhaj et al "Breast Cancer Ultrasound Images Analysis & Auto Segmentation of Lesions".
- [69] W. Leucht and D. Leucht, *Teaching Atlas of Breast Ultrasound*. New York: Thieme Medical, 2000, pp. 24–38.
- [70] J. Shan, H. D. Cheng and Y.X. Wang, "A novel automatic seed point selection algorithm for breast ultrasound images", *Proc. of the 19th International Conference on Pattern Recognition (ICPR 2008)*, Florida, USA, Dec 8-11, 2008.
- [71] Hwang, K.-H., H., Lee, J.G., Kim, J.H., Lee, H.-J. Om, K.-S., Yoon, M., and Choe, W. Computer aided diagnosis (CAD) of breast mass on ultrasonography and mammography. In *Proceedings of 7th International Workshop on Enterprise Networking and Computing in Healthcare Industry*, 2005, 187-189.
- [72] Burckhardt C. Speckle in Ultrasound B-Mode Scans. *IEEE Trans Son Ultrason* 1978; 25: 1– 6.
- [73] XRES@: adaptive enhancement of ultrasound images J. Jago, A. Collet-Billon, C. Chenal, J.-M. Jongand S. Makram-Ebeid.
- [74] *Speckle Noise Suppression Techniques for Ultrasound Images*.
- [75] Loupas, T., McDicken, W., & Allan, P.. An adaptive weighted median filter for speckle suppression in medical ultrasound images. *IEEE Transactions on Circuits and Systems*. 1989, 36(1), pp. 129-135.
- [76] *Speckle Reducing Anisotropic Diffusion* Yongjian Yu and Scott T. Acton, Senior member, IEEE.
- [77] *Digital Image Processing* by Rafael C. Gonzalez & Richard E. Woods.